Thesis for the degree of Doctor of Philosophy

Equilibrium Statistics of Channel-confined DNA

Erik Werner

Department of Physics
University of Gothenburg
Göteborg, Sweden 2015

Equilibrium Statistics of Channel-confined DNA
Erik Werner
ISBN 978-91-628-9555-6 (PDF)
ISBN 978-91-628-9556-3 (Print)

This thesis is electronically published, available at
http://hdl.handle.net/2077/40087

Front cover: Artist's impression of a DNA molecule confined to a nanochannel. Drawing by Karin Hartman.

Department of Physics
University of Gothenburg
SE-412 96 Göteborg
Sweden
Telephone: +46 (0)31-786 00 00

Printed by Kompendiet
Göteborg, Sweden 2015

Abstract

This thesis is devoted to the study of DNA molecules in nanochannels. In the last ten years, a large number of studies have been conducted wherein DNA molecules were confined to channels with a width of about 100 nm. These studies are motivated both by biotechnical applications, and by the potential for using nanochannels as a model system for studying the physics of confined DNA. The results of this thesis increase our understanding of the equilibrium statistics of such channel-confined DNA.

The results can be divided into three parts. In the first, we derive novel predictions for the extension statistics of channel-confined polymers. Specifically, we map out a phase diagram of scaling regimes for a polymer in a rectangular channel. Further, in an important special case known as the extended de Gennes regime, we show that the configurational statistics are equivalent to those of a one-dimensional model known as the weakly self-avoiding random walk. Exact results for that model yield rigorous predictions for the confined polymer.

In the second part we report experimental measurements of the extension statistics of confined DNA. We find that the measurements agree very well with theoretical predictions, except at low ionic strengths.

Finally, the third part of the thesis concerns the melting of DNA, i.e. the partial disassociation of its two strands at elevated temperatures. We solve a simple model of DNA melting and show that, within this model, channel confinement makes the transition to the molten state less abrupt, despite the fact that the order of the phase transition is unchanged by confinement.

List of papers

This thesis consists of an extended summary and the following appended research papers, hereafter referred to as [I], [II], [III], [IV], [V]:

Paper I
E. Werner and B. Mehlig. "Scaling regimes of a semiflexible polymer in a rectangular channel". *Physical Review E* **91** (5) (2015). DOI: 10.1103/PhysRevE.91.050601

Paper II
E. Werner and B. Mehlig. "Confined polymers in the extended de Gennes regime". *Physical Review E* **90** (6) (2014), p. 062602. DOI: 10.1103/PhysRevE.90.062602

Paper III
M. Alizadehheidari, E. Werner, C. Noble, M. Reiter-Schad, L. K. Nyberg, J. Fritzsche, B. Mehlig, J. O. Tegenfeldt, T. Ambjörnsson, F. Persson, and F. Westerlund. "Nanoconfined Circular and Linear DNA: Equilibrium Conformations and Unfolding Kinetics". *Macromolecules* **48** (3) (2015), pp. 871–878. DOI: 10.1021/ma5022067

Paper IV
V. Iarko, E. Werner, L. K. Nyberg, V. Müller, J. Fritzsche, T. Ambjörnsson, J. P. Beech, J. O. Tegenfeldt, K. Mehlig, F. Westerlund, and B. Mehlig. "Extension of nano-confined DNA: quantitative comparison between experiment and theory". *arXiv:1506.02241* (2015)

Paper V
E. Werner, M. Reiter-Schad, T. Ambjörnsson, and B. Mehlig. "Model for melting of confined DNA". *Physical Review E* **91** (6) (2015), p. 060702. DOI: 10.1103/PhysRevE.91.060702

Contributions

My contributions to the appended papers are:

- Paper [I]: I initiated the project and developed the theory. BM and I wrote the paper.
- Paper [II]: I initiated the project, wrote and analysed the computer simulations. I developed the theory, with help from BM. BM and I wrote the paper.
- Paper [III]: I developed the theory for the equilibrium statistics and wrote that section. I participated in the analysis of the experimental data.
- Paper [IV]: I participated in the discussions leading to the project, and in the planning of the experiments. I developed the theory and took part in the data analysis. BM and I wrote the lion's share of the paper, with help from the other authors.
- Paper [V]: I developed the theory, with help from TA and BM. I wrote and analysed the computer simulations. BM and I wrote the paper, with help from the other authors.

Additional Publications

During my time as a PhD student, I have co-authored three additional papers in the field of polymer theory, apart from the five that are included in the thesis. Refs. [A, B] are part of my Licentiate thesis [1]. Ref. [C] is not included in this thesis in order to make it more coherent, and because my contribution to it was not as substantial as for the other papers.

[A] E. Werner, F. Persson, F. Westerlund, J. O. Tegenfeldt, and B. Mehlig. "Orientational correlations in confined DNA". *Physical Review E* **86** (4) (2012), p. 041802. DOI: 10.1103/PhysRevE.86.041802 (cit. on pp. vi, 50).

[B] E. Werner, F. Westerlund, J. O. Tegenfeldt, and B. Mehlig. "Monomer Distributions and Intrachain Collisions of a Polymer Confined to a Channel". *Macromolecules* **46** (16) (2013), pp. 6644–6650. DOI: 10.1021/ma400464c (cit. on pp. vi, 30, 31, 33, 56, 57).

[C] M. Reiter-Schad, E. Werner, J. O. Tegenfeldt, B. Mehlig, and T. Ambjörnsson. "How nanochannel confinement affects the DNA melting transition within the Poland-Scheraga model". *arXiv:1505.01968. Accepted for publication in the Journal of Chemical Physics* (2015) (cit. on pp. vi, 64, 65).

Acknowledgements

First of all, I am profoundly thankful to Bernhard Mehlig for advising me throughout my years as a PhD student. Without your support I don't know how I would even have managed to get started.

Next, I would like to thank Fredrik Westerlund for grounding my ideas in reality, Jonas Tegenfeldt and Fredrik Persson for introducing me to a fascinating world of strings and blobs, and Tobias Ambjörnsson and Michaela Reiter-Schad for explaining the mysteries of melting. I have learned a lot from all of you.

I has been a pleasure to work together with master's students Ali Çakır, Vitalii Iarko and Toby St Clere Smithe. Thank you for your questions and for helping me answer mine.

I have also very much enjoyed sharing an office with Camilla, Joachim, Katarina, Marina and Jonas (not all at the same time). I'm sorry for ruining your workflow with questions, drumming and ice cream.

Alexander Björling, Jonas Einarsson and Marina Rafajlović have helped me with the proofreading of this thesis. If you find it legible and/or understandable it is largely their doing.

Huge thanks to Karin Hartman for the fantastic cover illustration, and to Per Eldenius for contributing to its design.

I am very grateful to the University of Gothenburg and the citizens of Sweden for allowing me to do research. It's been great fun.

Finally, as I don't have an Instagram account I'll take this opportunity to tell everyone what a fantastic family I have. #Eija #Tage #blessed

Contents

Part I
Introduction

Chapter 1. Introduction

This thesis concerns the statistical description of a very long molecule (a polymer) that is confined to a channel which is much narrower than the size of the molecule. The primary motivation is recent experiments where DNA molecules are inserted into channels with a width of about 100 nm. The research in this thesis attempts to explain the observations of these experiments, and to predict what is likely to happen in similar experiments which have not yet been carried out.

The experiments are interesting for three main reasons. First, understanding the behaviour of confined DNA molecules is of great biological interest. DNA plays a vital role in all living cells, in an environment where the molecule is always confined by the membrane of the cell or the nucleus. Nanochannel experiments provide a possibility to investigate the physics of DNA molecules in well-controlled environments and simple geometries, and can hopefully help us understand the configurations of a DNA molecule in a cell. Such experiments have revealed that confinement significantly alters the properties of DNA [2, 3]. Second, there are biotechnical applications where DNA is confined in channels, e.g. genomic mapping [4–10] and the study of DNA-protein interactions [11–16]. To optimise these systems, it is necessary to understand the configurations of the molecule, and to be able to predict the effect of changing the system parameters. Third, DNA molecules in nanochannels are an excellent model system for polymer theory, as DNA are long and well-characterised, and standard techniques for handling, manipulating and visualising single DNA molecules have been developed by biologists. Similarly, the development of clean room patterning techniques allows for the manufacturing of well-defined geometries down to the nanometre scale [2, 5, 17]. This has enabled the testing of old polymer theory predictions [18–23], and has raised a number of new questions regarding single-polymer statistics [24–27].

Finally, one of the most useful aspects of polymer theory is that its results are not specific to a certain molecule. Thus the methods of this thesis are not only applicable to DNA in nanochannels, but to a large class of molecules. In fact, similar experiments to the ones with DNA that motivate this thesis have been performed with other biological polymers [16, 20, 28]. The equivalence between different models can also be used to simplify calculations and simulations. As long as a simpler model of a molecule satisfies a small number of conditions, then results which are derived for the simple model are expected to hold also for DNA. The equivalence between different polymers is discussed in detail in Chapters 2 and 3, and used extensively in Chapter 4 and Refs. [I, II].

1.1 Outline

The rest of the thesis is structured as follows: Chapter 2 introduces the wormlike chain model of a DNA molecule, and discusses its parameters. In Chapter 3 I re-derive some standard results for the equilibrium statistics of an unconfined polymer, and discuss the equivalence between different polymer models.
Chapter 4 presents the results of Papers [I, II], which are new predictions for the extension statistics of a polymer confined to a channel.
Chapter 5 presents the results of Papers [III, IV], which consist of comparisons between experimental extension measurements and the theoretical predictions of Chapter 4.
Chapter 6 introduces the concept of DNA melting and presents the results of Paper [V], which describes how confinement in a channel affects the melting statistics of a simple model of DNA.
Finally, Chapter 7 summarises the thesis and discusses some possible future directions of research.

Chapter 2. Modelling DNA

The chemical and geometric structure of a DNA molecule is highly complex (see Fig. 2.1). The purpose of this chapter is to introduce a simplified model of DNA that ignores the chemical details of the molecule in order to afford a simple mathematical description. The justification for these simplifications follows in the next chapter. This model is fully specified by three parameters: First, the *contour length* L, i.e. the distance from one end to the other, measured along the molecule. Second, the *persistence length* ℓ_{P}, which measures the stiffness of the molecule. Third, the *effective width* w_{eff}, which quantifies the repulsive interactions between different parts of the molecule. Below we discuss how the values of these parameters are believed to depend on the ionic conditions of the solution surrounding the molecule.

2.1 The wormlike chain

The most common model for the physical properties of a DNA molecule in ionic solution is the *wormlike chain* or Kratky-Porod model [30–32]. It is illustrated in Fig. 2.2. This model ignores details such as the relative positions and orientation of the individual atoms, and assumes that the configuration of the molecule is fully specified by a smooth curve $\mathbf{r}(s)$. Here, the parameter s measures the contour distance from the beginning of the polymer. Let $\mathbf{t}(s) = \partial_s \mathbf{r}(s)$ denote the unit tangent vector of the curve. The curve has a fixed contour length $L = \int_0^L |\mathbf{t}(s)|\, ds = \int_0^L ds$. The smoothness of the curve is enforced by a bending energy which depends on the persistence length ℓ_{P} and the local curvature $|\partial_s \mathbf{t}(s)|^2$ as

$$\frac{E}{k_{\mathrm{B}}T} = \int_0^L \frac{\ell_{\mathrm{P}}}{2} \left|\partial_s \mathbf{t}(s)\right|^2 ds. \tag{2.1}$$

Here, k_B is *Boltzmann's constant* and T the temperature of the solution.

The wormlike chain model of DNA has been tested by a number of different experimental techniques [31, 33], showing that it is a good model of DNA, except when subjected to very high forces [34, 35], or in the presence of positive polyvalent ions [36]. The contour length can be directly computed from the lateral distance between base pairs as $L = (\text{Number of base pairs}) \times 0.34\,\text{nm}$ [29]. Measurements in monovalent solutions at physiological ion concentrations usually find a persistence

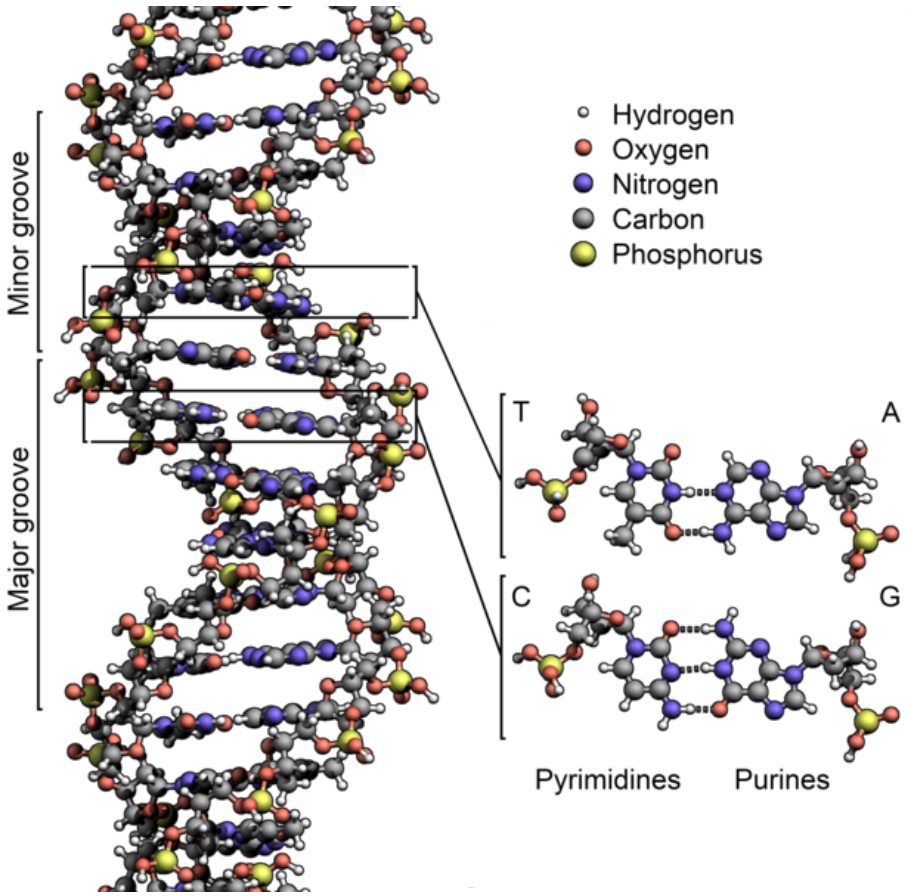

Figure 2.1: A sketch of the chemical structure of the DNA molecule (in the most common conformation, known as B-DNA), with complementary bases surrounded by a double-helical sugar-phosphate backbone. The diameter of the helix is 20 Å, and it does a full turn once every 10.5 base pairs [29]. Picture by Richard Wheeler, retrieved from http://commons.wikimedia.org/wiki/File:DNA_Structure%2BKey%2BLabelled.pn_NoBB.png, and reproduced under a Creative Commons license.

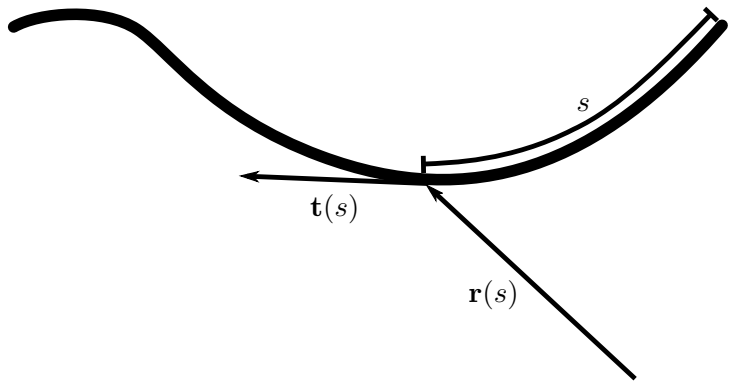

Figure 2.2: An illustration of a wormlike chain.

length in the range $\ell_P \approx 45$–$50\,\mathrm{nm}$ (see Table 1 of Ref. [37] for a summary of many different experimental results). However, there is no consensus regarding how the persistence length depends on the conditions of the surrounding solution.

At high ionic strengths, the stiffness is mechanical in origin – bending the molecule increases the energy because it requires the relative positions of atoms to shift from their potential minima. At low ionic strengths, the stiffness is increased by electrostatic repulsion between neighbouring segments of the molecule. The DNA molecule has a negative charge of two elementary charges per base-pair, or $2e$ per $3.4\,\text{Å}$ of contour length [38]. Because of this electric charge, DNA segments which approach each other in space are strongly repelled. However, experiments are conducted in ionic solution. The positive ions in the solution are attracted to the negative DNA, which screens the charge and weakens the repulsion. The electrostatic interaction is often approximated by Debye-Hückel theory [32]. Within this theory, the effect of the solution is captured by a single number, the ionic strength

$$I_s = \frac{1}{2}\sum_i c_i z_i^2. \tag{2.2}$$

Here, the sum runs over all ionic species in the solution; c_i is the concentration of ion species i and z_i its valence. Debye-Hückel theory predicts that positive ions form a condensation cloud around the DNA, leading to short-ranged repulsion between DNA segments [39]. The

range of the repulsion can be estimated by the Debye length [39, 40]:

$$\lambda_{\mathrm{D}} = (8\pi\lambda_{\mathrm{B}} N_{\mathrm{A}} I_{\mathrm{s}})^{-1/2}\,. \tag{2.3}$$

Here $\lambda_{\mathrm{B}} \approx 0.7\,\mathrm{nm}$ is the Bjerrum length of water, and N_{A} is Avogadro's constant.

Since the range of the electrostatic repulsion increases with decreasing ionic strength, it is clear that the persistence length must also increase. But there are three competing theories for the functional dependence of the persistence length upon the ionic strength. The classic theory of Odijk, Skolnick and Fixman [41, 42] predicts that the measured persistence length is a sum of two terms: a 'bare' persistence length $\ell_{\mathrm{P}}^{(0)}$, and an electrostatic persistence length $\ell_{\mathrm{P}}^{(\mathrm{el})}$ given by

$$\ell_{\mathrm{P}}^{(\mathrm{el})} = \lambda_{\mathrm{B}}\lambda_{\mathrm{D}}^2\nu^2/4, \tag{2.4}$$

where ν is the effective line charge density of DNA, which differs from the intrinsic line charge density of $2e$ per base pair, since it includes the effect of counterions from the solution associating to the DNA and partially neutralising the charge. According to Manning's condensation theory [43], for a strongly charged molecule like DNA, counterions will condense onto the molecule until the effective line charge is reduced to one electron charge per Bjerrum length, i.e. $\nu = 1/\lambda_{\mathrm{B}}$. Inserting this value into Eq. (2.4) and assuming $\ell_{\mathrm{P}}^{(0)} = 50\,\mathrm{nm}$ yields [44]

$$\ell_{\mathrm{P}} = 50\,\mathrm{nm} + \frac{0.0324\,\mathrm{M}}{I_{\mathrm{s}}}\,\mathrm{nm}. \tag{2.5}$$

Ten years ago, Dobrynin and Rubinstein pointed out that the quadratic dependence of $\ell_{\mathrm{P}}^{(\mathrm{el})}$ upon λ_{D} follows from the assumption that the configuration of the molecule can be approximated locally by a section of a circle [45]. Relaxing this assumption instead yields $\ell_{\mathrm{P}}^{(\mathrm{el})} \propto \lambda_{\mathrm{D}}$. By fitting this scaling to experimental estimates of the persistence length, Dobrynin [46] proposed the empirical formula

$$\ell_{\mathrm{P}} = 46\,\mathrm{nm} + \frac{1.9\,\mathrm{M}^{1/2}}{I_{\mathrm{s}}^{1/2}}\,\mathrm{nm}. \tag{2.6}$$

In a later publication, Gubarev, Carrillo and Dobrynin [47] conclude that at high ionic strengths Eq. (2.5) is correct after all. Nevertheless, we

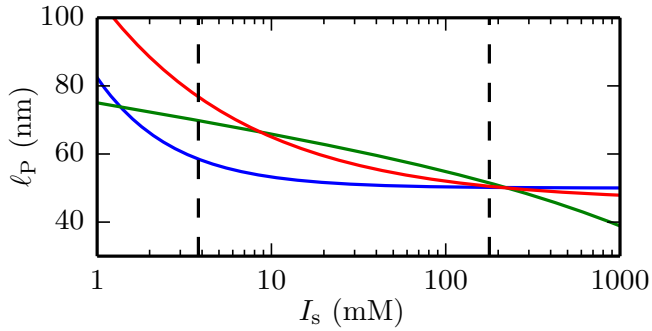

Figure 2.3: A comparison of different theories for the dependence of the persistence length upon the ionic strength. Blue: OSF theory, Eq. (2.5). Red: Dobrynin's formula, Eq. (2.6). Green: Manning's theory, Eq. 25 of Ref. [51]. Dashed lines indicate the range of ionic strengths explored in Paper [IV].

have adopted Eq. (2.6) as a baseline expression for the persistence length when comparing extension measurements to theoretical predictions in Paper [IV]. The reason is that this formula has been used in a number of recent studies [26, 27, 48, 49] and appears to reproduce most experimental measurements reasonably well [37, 44, 46, 50]. However, there is still considerable uncertainty regarding the dependence of ℓ_P on the ionic strength, as estimates vary considerably between different studies [37, 50].

Apart from these theories which separate the persistence length into a sum of two terms, one mechanical and one electrostatic, there is also a theory by Manning [51]. This theory attempts to separate the mechanical and the electrostatic persistence lengths by analysing a hypothetical molecule which is identical to real DNA, except that its phosphate groups are neutral rather than negatively charged. Experimental fits yield a mechanical persistence length as low as 7 nm. Interestingly, within this theory the effect of electrostatic repulsion on the persistence length is not additive as in Eqs. (2.5)–(2.6).

The three theories for the persistence length are compared in Fig. 2.3. The figure shows that the three theories agree very well for ionic strengths of about 200 mM,[1] but disagree at lower ionic strengths.

[1]The agreement is a consequence of the large number of measurements at these ionic strengths, which constrain the fits inherent in the three expressions for ℓ_P.

2.2 Non-neighbour interactions

In the previous subsection we described the representation of the DNA molecule and the energy required to bend the molecule locally. Yet it remains to define the interaction between non-adjacent sections of the molecule. As discussed above, two segments which approach must repel each other. Since the interaction is short-ranged, it can be approximately described as hard-core repulsion with an *effective width* w_{eff} which depends on the ionic strength.

The standard calculation of the effective width was carried out by Stigter [52]. He assumed that the effective width could be determined by treating two non-adjacent DNA segments as thin, charged cylinders, and matching the second virial coefficient of their interaction [53, §74] to that of two self-avoiding cylinders [54]. The rationale behind this matching is explained in Section 3.2.1. The result of Stigter's calculation is tabulated in Ref. [55], and we have used these results as the baseline for the effective width when comparing experiments in Paper [IV]. It must be noted, however, that there are a number of untested assumptions entering into the calculation. First, it is assumed that each cylinder has an intrinsic width of 1.2 nm, but this number has an uncertainty of about 20% [52]. Additionally, the assumed effective line charge of the cylinders is based on measurements in NaCl-solution, and does not apply in solutions with other ions [56]. In view of this fact, it is particularly problematic that most experimental tests of Stigter's formula have been performed in NaCl-solution [57].

2.3 Effect of dyes

In order to make the DNA visible in a fluorescence microscope, the molecule must be stained with a dye. This changes the mechanical properties of the molecule. In single-molecule experiments, YOYO-1 and similar dyes are most commonly used [5, 58]. These dyes consist of two aromatic subunits, bridged by a linker. When the dye is bound to DNA, the two subunits intercalate between base pairs, enclosing two base pairs between them [5].

The most obvious effect of the intercalation is that it increases the contour length of the molecule. The elongation is commonly assumed to increase in proportion to the number of dye molecules bound. Estimates

for the increase in contour length per molecule range from about 0.4 nm to 0.5 nm, with large uncertainties for the individual estimates [59, 60].

In order to bind strongly to the negatively charged DNA molecule, the dyes are positively charged – each YOYO-1 molecule carries four positive charges. The resulting decrease in negative charge as the dye binds to the DNA decreases the charge of the molecule, thus potentially reducing the repulsion between segments and decreasing the effective width. The magnitude of this effect is not known.

Finally, the intercalating dye might change the persistence length of the DNA, but the effect is hard to estimate. Different experiments show contradictory results, some indicating that the persistence length decreases sharply at high staining [61, 62], others that it is essentially independent of staining [60].

To summarise, the effect of staining on the physical parameters of the DNA-dye complex is not well understood. This uncertainty makes it difficult to quantitatively interpret experiments where a high staining ratio is used. For our baseline scenario when comparing to experiments, we assume that the contour length is increased by 0.44 nm per dye molecule (following Ref. [26]) but that the persistence length and the effective width remain unchanged by staining.

2.4 Ionic strength calculations

The theories discussed above for the physical parameters of DNA are all given as functions of the ionic strength I_s. Most single-molecule DNA experiments in nanochannels are performed in TBE buffer, at a concentration ranging from 0.02×TBE to 5×TBE [2, 5, 63]. For these buffers, calculating the ionic strength requires one to solve for the equilibrium concentration of ions. This calculation is explained in the supplemental material of Paper [IV]. The calculation presented there also takes into account the effect of β-mercaptoethanol (BME), a weak acid that is added to the solution in order to inhibit photonicking of the dye molecules.

2.5 Summary

To summarise, while it is believed that a DNA molecule can be described by the self-avoiding wormlike chain model under fairly general conditions,

Table 2.1: Numerical values for the ionic buffer strength I_s, the persistence length ℓ_P, and the effective width w_{eff} for the different concentrations of the TBE buffer employed in Papers [III, IV] (the effect of adding 3% BME has been taken into account).

$x\times$TBE	0.05	0.1	0.5	2	2.5	5
I_s[mM]	3.81	7.42	24.9	78.4	95.5	178.0
ℓ_P[nm]	77	68	58	53	52	51
w_{eff}[nm]	26	18	10	6.2	5.7	4.6

there is considerable uncertainty regarding how the parameters ℓ_P and w_{eff} defining the model depend on the buffer conditions, and upon the dye staining ratio. In order to obtain definite prediction against which to compare the experiments described in Chapter 5, we assume as a baseline scenario that ℓ_P is given by Dobrynin's empirical formula [46] [Eq. (2.6)], and w_{eff} by Stigter's calculation [52, 55] (see discussion above). For the buffer conditions that have been employed in Papers [III, IV], the resulting parameter estimates are tabulated in Table 2.1.

Chapter 3. Unconfined polymers

We saw in the previous chapter how a DNA molecule can be described by the self-avoiding wormlike chain model of a polymer, with parameters L, ℓ_{P}, and w_{eff} (contour length, persistence length, and effective width).

In this chapter we re-derive some standard results for the extension statistics of such a polymer. In the next chapter, we build on these results to derive the extension statistics of a polymer confined to a channel.

3.1 Ideal polymers

First we consider the special case of a wormlike chain with $w_{\mathrm{eff}} = 0$, i.e. when it is impossible for non-neighbouring segments to interact. Polymers for which this non-interacting property holds are called ideal polymers.

3.1.1 Orientational correlations

The ideal wormlike chain is stiff at short length scales but flexible at large lengths scales. This is quantified by the orientational or tangent-tangent correlation function

$$C(s_1, s_2) \equiv \langle \mathbf{t}(s_1) \cdot \mathbf{t}(s_2) \rangle \,. \tag{3.1}$$

The brackets denote an ensemble average, and $\mathbf{t}(s)$ is the tangent vector at contour distance s, illustrated in Fig. 2.2. From Eq. (2.1) it follows that for the ideal and unconfined wormlike chain the orientational correlation function has the simple form [64]

$$C(s_1, s_2) = \exp\left(-\frac{|s_2 - s_1|}{\ell_{\mathrm{P}}}\right). \tag{3.2}$$

Thus, if the contour distance $|s_2 - s_1|$ is much smaller than the persistence length, the tangent vectors have a strong tendency to point in the same direction. If on the other hand the contour distance is much larger than the persistence length, the tangent vectors are uncorrelated, and in fact independent [64]. A polymer which is stiff at short length scales and flexible at large length scales is called a semiflexible polymer [32].

3.1.2 Extension

A common way to characterise the size or extension of a polymer is the root mean square of its end-to-end vector $\mathbf{r} \equiv \mathbf{r}(L) - \mathbf{r}(0)$

$$\left\langle |\mathbf{r}|^2 \right\rangle^{1/2} = \left\langle |\mathbf{r}(L) - \mathbf{r}(0)|^2 \right\rangle^{1/2}. \tag{3.3}$$

Rewriting $\mathbf{r} = \int_0^L ds\mathbf{t}(s)$, inserting it into Eq. (3.3) and using Eqs. (3.1)–(3.2) yields [64]

$$\left\langle \mathbf{r}^2 \right\rangle = \iint_0^L ds_1 ds_2 C(s_1, s_2) = 2\ell_\mathrm{P}^2 \left(e^{-L/\ell_\mathrm{P}} - 1 + L/\ell_\mathrm{P} \right). \tag{3.4}$$

In the limit $L \ll \ell_\mathrm{P}$ Eq. (3.4) simplifies to $\left\langle \mathbf{r}^2 \right\rangle^{1/2} = L$, the expected value for a stiff rod. In the opposite limit $L \gg \ell_\mathrm{P}$, we find $\left\langle \mathbf{r}^2 \right\rangle^{1/2} = \sqrt{2L\ell_\mathrm{P}}$.

The fact that the rms end-to-end distance of a long polymer grows as the square root of its contour length is a consequence of the fact that two tangent vectors are independent if the contour separation between them is large. Since the end-to-end vector is the sum of many such independent contributions, its statistics are akin to those of a random walk of independent steps. In particular, the distribution of end-to-end vectors tends to a Gaussian distribution with mean zero and variance $\sigma^2_\mathrm{ideal} = 2L\ell_\mathrm{P}$ [65],

$$P_\mathrm{ideal}(\mathbf{r}) = \left(\frac{3}{4\pi L \ell_\mathrm{P}} \right)^{-3/2} \exp\left(-\frac{3\mathbf{r}^2}{4L\ell_\mathrm{P}} \right), \; L \gg \ell_\mathrm{P}. \tag{3.5}$$

The analogy with a random walk can be used to simplify the description of the polymer: For a long wormlike chain ($L \gg \ell_\mathrm{P}$), the statistics of the end-to-end vector are identical to those of a random walk of $N = L/\ell_\mathrm{K}$ independent steps of length $\ell_\mathrm{K} = 2\ell_\mathrm{P}$. In the polymer context, this model is called the freely jointed or random flight chain, and the step length ℓ_K is called the *Kuhn length* [32].

3.2 Self-avoiding polymers

In the previous section, we saw that it is possible to derive closed-form expressions for the extension statistics of the ideal wormlike chain. As a

rule, this is not possible for self-avoiding polymers[1]. However, there are a number of approximate theories for the extension statistics of a self-avoiding polymer [66, 67]. The simplest such theory, usually called Flory theory [68], is discussed below. We begin by deriving the implications of this theory for the extension statistics of the self-avoiding wormlike chain. Then we describe how the theory can be applied to other polymer models. Finally we discuss the correctness of its predictions.

3.2.1 Flory theory for the self-avoiding polymer

One way to get a statistically accurate ensemble of self-avoiding polymers is to start with an ensemble of ideal polymers, and then remove any members of the ensemble in which two or more segments overlap. It follows from this procedure that the probability distribution for the end-to-end vector of the self-avoiding polymer can be written

$$P(\mathbf{r}) \propto P_{\text{ideal}}(\mathbf{r})A(\mathbf{r}), \tag{3.6}$$

where P_{ideal} is given by Eq. (3.5) and the acceptance rate $A(\mathbf{r})$ is defined as the fraction of ideal polymers with end-to-end vector $\mathbf{r}$ which are free of overlaps between segments. The acceptance rate $A(\mathbf{r})$ can be estimated by a mean-field argument originally due to Flory [69] and generalised to semiflexible polymers by Schaefer et al. [70]: Divide the polymer into $N = L/\ell_{\text{K}}$ Kuhn length segments and estimate the probability p that any pair of segments overlap by assuming that the two segments are randomly oriented and positioned within a region of volume $V = r^3$, where $r \equiv |\mathbf{r}|$ is the end-to-end distance. This probability can be written $p = v/V$, where v is called the *excluded volume* of a segment. Assuming that the excluded volume of a persistence length segment is similar to that of a thin rod yields $v = (\pi/2)\ell_{\text{K}}^2 w_{\text{eff}}$ [54, 71], where we assume that $\ell_{\text{K}} \gg w_{\text{eff}}$. Since there are $N(N-1)/2 \approx N^2/2$ segment pairs that must not overlap, the mean field estimate for the acceptance rate is

$$A(r) \approx (1-p)^{N^2/2} \approx \exp(-N^2 p/2), \tag{3.7}$$

[1]For a channel-confined polymer in the so-called extended de Gennes regime, an exception to this rule is derived in Paper [II] (see also Section 4.2).

where we assume that $p \ll 1$. Inserting Eq. (3.5) and Eq. (3.7) into Eq. (3.6) and taking the logarithm yields[2]

$$\log P(r) = \text{const.} - \frac{3r^2}{2L\ell_\mathrm{K}} - \frac{\pi L^2 w_\mathrm{eff}}{4r^3}. \tag{3.8}$$

Recall that the Kuhn length $\ell_\mathrm{K} = 2\ell_\mathrm{P}$ is the step size of the equivalent freely-jointed chain. The Flory estimate of the extension is given by the end-to-end distance which maximises Eq. (3.8). We find

$$R_\mathrm{MF} \approx L^{3/5} \ell_\mathrm{K}^{1/5} w_\mathrm{eff}^{1/5}, \tag{3.9}$$

where $R = |r|$ denotes the average end-to-end distance. Further, the sign "$\approx$" means that we drop numerical prefactors of order unity. Note that the mean-field theory predicts that the extension of a self-avoiding polymer grows with contour length as $R \propto L^{3/5}$, compared to $R \propto L^{1/2}$ for the ideal polymer.

Eq. (3.8) also yields a prediction for the variance of the end-to-end distance:

$$\sigma^2_\mathrm{MF} \approx L\ell_\mathrm{K}. \tag{3.10}$$

Thus, except for a possible change of prefactor, mean-field theory predicts that the end-to-end distance of the self-avoiding chain has the same variance as the ideal chain.

Model independence

So far, the discussion has been restricted to a single polymer model, the self-avoiding wormlike chain. Yet the results we have derived are insensitive to the details of the model. In the mean-field expression for $P(r)$ [Eq. (3.8)], the three parameters L, ℓ_K (or ℓ_P) and w_eff of the self-avoiding wormlike chain appear in only two combinations:

1. $\sigma^2_\mathrm{ideal} = L\ell_\mathrm{K}$, the variance of the corresponding ideal chain.
2. $\mathcal{V} = \pi L^2 w_\mathrm{eff}/2$, which can be interpreted as the volume V for which the average number of overlaps is approximately one.

[2]Considering also the volume in phase space corresponding to an end-to-end distance r yields $P_\mathrm{ideal}(r) \propto r^2 P_\mathrm{ideal}(\mathbf{r})$. In Eq. (3.8) we disregard the factor r^2, which does not influence the conclusions.

The two parameters can be combined into a dimensionless number which quantifies the importance of self-avoidance,

$$z = \mathcal{V}/\sigma_{\text{ideal}}^3 = (\pi/2)L^{1/2}w_{\text{eff}}/\ell_{\text{K}}^{3/2}. \tag{3.11}$$

Eq. (3.8) for the probability distribution of the extension can be rewritten in terms of σ_{ideal} and z:

$$\log P(r) \approx \text{const.} - (r/\sigma_{\text{ideal}})^2 - \frac{z}{(r/\sigma_{\text{ideal}})^3}. \tag{3.12}$$

The number z has a simple interpretation as the average number of overlaps for a polymer in the initial ideal ensemble. If $z \ll 1$ then self-avoidance has little influence on the polymer statistics. If on the other hand $z \gg 1$ then self-avoidance has a profound influence on the statistics, leading to the scaling $R_{\text{MF}} \propto L^{3/5}$ derived above.

Since the predictions of the mean-field theory only depend on the polymer model through the parameters σ_{ideal} and $\mathcal{V}$ (or z), they apply equally well to other polymer models. The theory requires only that it is possible to make a clear distinction between neighbour and non-neighbour interactions. Disregarding the latter yields the corresponding ideal polymer model. As for the wormlike chain it is always possible to define a Kuhn length ℓ_{K} such that a long ideal polymer has a variance of $\sigma_{\text{ideal}}^2 = N\ell_{\text{K}}^2$ The effect of the non-neighbour interactions can be captured by a single parameter, the excluded volume v between two Kuhn length segments. Assume that two segments separated by a vector $\Delta\mathbf{r}$ have an interaction energy $U(\Delta\mathbf{r})$. Then, the excluded volume is defined as [67][3]

$$v = \int d\Delta\mathbf{r} \left[1 - \exp\left(-\frac{U(\Delta\mathbf{r})}{kT}\right)\right]. \tag{3.13}$$

If the interaction depends not only on the separation between segments but also on their internal configurations and relative orientation, then the definition of v must include an average over these factors also.

In terms of the excluded volume v and the number of segments N, the parameters $\mathcal{V}$ and z are given by $\mathcal{V} = N^2 v$ and $z = \sqrt{N}v/\ell_{\text{K}}^3$.[4]

[3] A comparison with the virial expansion for non-ideal gases [53, §74] shows that the excluded volume is related to the second virial coefficient B by $v = 2B$.

[4] The parameter z is usually defined as $z = (3/(2\pi))^{3/2} v N^{1/2} b^{-3/2}$ [72]. For simplicity, we drop the prefactor.

Note that according to Eq. (3.13), v turns negative if the interaction is predominantly attractive. In this case, the polymer collapses to a compact globule which cannot be described by any of the theories described in this thesis [32].

3.2.2 Accuracy of Flory theory

The mean-field theory that we have presented above makes three predictions:

1. The statistics do not depend on the details of the model, but only on the two parameters $\sigma_{\text{ideal}} = \sqrt{N}\ell_{\text{K}}$ and $z = \sqrt{N}v/\ell_{\text{K}}^3$.

2. The average extension scales as

$$R_{\text{MF}} \approx \sigma_{\text{ideal}} z^{1/5} = N^{3/5}\ell_{\text{K}}^{2/5} v^{1/5}. \tag{3.14}$$

3. The standard deviation of the extension scales as

$$\sigma_{\text{MF}} \approx \sigma_{\text{ideal}} = \sqrt{N}\ell_{\text{K}}. \tag{3.15}$$

We now discuss these in turn.

1.

Only having to define two parameters in order to characterise the statistics of any polymer is of course a huge simplification. Nevertheless, this two-parameter model is thought to capture the essential aspects of most polymers, in particular the extension statistics of a long polymer [32, 66, 67]. For polymers obeying $v \ll \ell_{\text{K}}^3$ the two-parameter model correctly describes also the cross-over from ideal to self-avoiding scaling [73, 74]. Since the wormlike chain with $w_{\text{eff}} \ll \ell_{\text{K}}$ obeys this condition, the two-parameter model is excellent as a model for DNA at high ionic strengths.

In fact, the very possibility of modelling DNA as a self-avoiding wormlike chain follows from the accuracy of the two-parameter model – recall from Chapter 2 that the actual interaction between non-neighbouring segments is not hard-core repulsion but screened electrostatic repulsion. The effective width of DNA is *defined* by matching the excluded volume (or the second virial coefficient) of the physical molecule to that of a

cylinder of length ℓ_K and width $w_{eff} \ll \ell_K$, for which $v = \pi \ell_K^2 w_{eff}/2$ [54, 71].

The equivalence between different models can also be exploited in order to simplify the description of the polymer. For example, in the calculations and simulations described in the next chapter we sometimes model the DNA molecule as a freely jointed chain of self-avoiding beads (see Fig. 4.3). As long as $L \gg \ell_K$, this very simple model should yield an equally accurate description of DNA as the wormlike chain.

2.

Given the simplicity of the mean-field calculation above, the predictions of Eqs. (3.9) and (3.14) are surprisingly accurate. More advanced perturbation calculations [67], which agree very well with simulations [75], yield

$$R \approx \sigma_{ideal} z^{0.176} \approx N^{0.588} \ell_K^{0.472} v^{0.176} \approx L^{0.588} \ell_K^{0.236} w_{eff}^{0.176}. \qquad (3.16)$$

Note that the scaling exponent for the contour length differs from the mean-field prediction by only 2%. Intriguingly, the corresponding mean-field prediction for a two-dimensional polymer is thought to be exact [75]. Mean-field theory predicts

$$R_{2D} \approx \sigma_{ideal} z^{1/4} = N^{3/4} \ell_K^{1/2} a^{1/4}. \qquad (3.17)$$

Here, a is the excluded area of a Kuhn length segment of the two-dimensional polymer, defined in the same way as the excluded volume in three dimensions. $\sigma_{ideal} = \sqrt{N}\ell_K$ and $z = Na/\ell_K^2$ are also defined analogously to the three-dimensional polymer. Eq. (3.17) is thought to describe correctly the statistics of a two-dimensional polymer in the limit $z \gg 1$ [67, 75].

3.

Eqs. (3.10) and (3.15) are believed to underestimate the variance significantly, both in two and three dimensions. They predict that the standard deviation of the polymer extension is significantly smaller than its average. Yet this contradicts a fundamental principle of scale invariance, which says that the self-avoiding polymer in the limit $z \gg 1$ only has a single macroscopic length scale [67]. It follows that $\sigma \approx R$

[76]. The existence of a single length scale also justifies our use of the end-to-end distance as a measure of the polymer extension – the statistics of other observables such as the radius of gyration must obey the same scaling as Eq. (3.16), differing only in the prefactor.

3.3 Contour length scales

We have seen that the extension statistics of the self-avoiding wormlike chain exhibits three scaling regimes:

1. If $L \ll \ell_{\mathrm{P}}$ then the polymer is rodlike, $R \propto L$.
2. If $L \gg \ell_{\mathrm{P}}$ and $z \ll 1$ then the polymer exhibits random-walk scaling, $R \propto L^{1/2}$.
3. If $L \gg \ell_{\mathrm{P}}$ and $z \gg 1$ then the extension is dominated by self-avoidance, $R \propto L^{\nu}$, where $\nu = 0.588 \approx 3/5$.

An alternative way of distinguishing between these regimes is to consider the relation between the contour length scales of the polymer [I]. The ideal polymer has two length scales, L and ℓ_{K} (or ℓ_{P}, which differs from ℓ_{K} by a prefactor only). When self-avoidance is included a third length scale appears: l_{cc}, the average contour length separation between overlaps. l_{cc} is given by the contour length such that $z = 1$,

$$\frac{\pi l_{\mathrm{cc}}^{1/2} w_{\mathrm{eff}}}{4\ell_{\mathrm{K}}^{3/2}} = 1 \Leftrightarrow l_{\mathrm{cc}} \approx \frac{\ell_{\mathrm{K}}^3}{w_{\mathrm{eff}}^2}. \tag{3.18}$$

Since $w_{\mathrm{eff}} \ll \ell_{\mathrm{K}}$, it is always the case that $\ell_{\mathrm{K}} \ll l_{\mathrm{cc}}$. The three contour length scales can therefore be related in three ways,

1. $L \ll \ell_{\mathrm{K}} \ll l_{\mathrm{cc}}$.
2. $\ell_{\mathrm{K}} \ll L \ll l_{\mathrm{cc}}$.
3. $\ell_{\mathrm{K}} \ll l_{\mathrm{cc}} \ll L$.

These three relationships directly correspond to the three scaling regimes discussed at the beginning of this section.

In the next chapter, we discuss the effect of channel confinement on the extension statistics. Under confinement, additional contour length scales appear which can be used to characterise different scaling regimes.

Part II
Present work

The research of this thesis concerns the conformational statistics of a DNA molecule confined to a channel. The research can be divided into three parts, corresponding to Chapters 4, 5 and 6.
Chapter 4 contains new predictions for the extension statistics of a polymer confined to a channel.
Chapter 5 consists of comparisons between experimental extension measurements and the theoretical predictions of Chapter 4.
Chapter 6 describes how channel confinement affects the melting statistics of a simple model of DNA.

Chapter 4. Channel confinement

This chapter describes the results of Papers [I] and [II]. Here we derive new predictions for the extension statistics of a channel-confined, semiflexible polymer. Paper [I] is summarised in Section 4.1. In this paper we show that a polymer in rectangular confinement exhibits different behaviours, depending on how the geometry of the channel is related to the parameters ℓ_{K} and w_{eff} of the polymer. Using similar mean field arguments as in Section 3.2.1, we derive predictions for the extension statistics in the different *scaling regimes*. The results are important in light of the fact that while many experimental studies of confined DNA are performed in rectangular channels [16, 18, 19, 24, 26, 49, 77–79], most simulation and theoretical studies are restricted to channels with square cross-sections, $D_{\mathrm{W}} = D_{\mathrm{H}}$ [80–85].

Paper [II] is summarised in Section 4.2. Here we focus on one of the scaling regimes, called the extended de Gennes regime. We show that in this regime it is possible to map the configurational statistics to a one-dimensional random walk model. Exploiting the results of this model we can not only prove that the mean-field scaling for the extension statistics is exactly correct, but also derive rigorous bounds for the prefactors. Further, the one-dimensional model exhibits a universal

scaling law which applies also to microscopic observables. In other words any results that have been derived for one set of parameters (e.g. by simulations of either the 3D or the 1D model) can be directly translated to any other set of parameters within the extended de Gennes regime.

4.1 Rectangular channels

We describe in the previous chapter how an unconfined self-avoiding polymer such as DNA forms a *blob* with an approximate extension given by Eq. (3.9). Now consider what happens if such a polymer is confined to a rectangular channel where both sides of the cross-section are significantly shorter than the average extension of the unconfined polymer. In order to avoid overlaps between different segments, the extension of the polymer must increase significantly beyond its unconfined value. In fact, in order to avoid that the local segment concentration increases without bound as $L \to \infty$, the mean extension R must increase in proportion to the contour length in this limit [68]. It follows that a long polymer can be divided into a number of non-interacting segments, and therefore also the variance of the extension grows as $\sigma_{\mathrm{R}}^2 \propto L$. The question that we pose in Paper [I] is how the extension statistics of a long polymer depends on the other parameters of the problem, i.e. the Kuhn length ℓ_{K}, the width w_{eff}, the channel width D_{W} and the channel height D_{H}.

As we discussed at the end of the previous chapter, for an unconfined polymer the functional dependence of the extension upon the parameters of the problem exhibits different scaling regimes which can be distinguished by the relationships between its contour length scales. We show in Paper [I] that the same is true for the confined polymer, and that the problem is complicated by the appearance of two new length scales. These are l_{cw}, the typical contour length separation between collisions with the vertical walls of the channel, and l_{ch}, the typical contour length separation between collisions with the floor and ceiling of the channel. Without loss of generality we assume throughout this chapter that $D_{\mathrm{W}} \geq D_{\mathrm{H}}$, from which it follows that $l_{\mathrm{cw}} \geq l_{\mathrm{ch}}$. Further we restrict the discussion to the case where the full contour length L is the largest of the length scales, so that the linear scaling of R and σ_{R}^2 with L holds. In this case, there are 6 ways to order the length scales, leading to the 6 scaling regimes listed in Table 4.1 and sketched in Fig. 4.1. Regimes Ia, Ib and Ic have been grouped together, as our

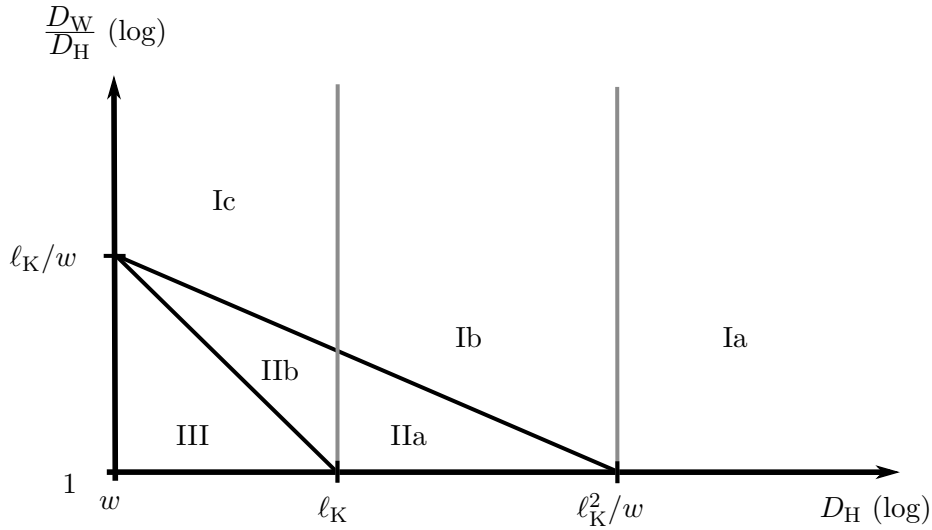

Figure 4.1: Phase diagram of different scaling regimes for the extension statistics of a semi-flexible polymer confined to a channel with a rectangular cross-section.

analysis shows that the scaling of the extension statistics are identical in these regimes. The same is true of regimes IIa and IIb. Regime III has been described previously elsewhere [83, 86, 87]. This regime can in fact be subdivided into two regimes, since an additional length scale g called the global persistence length [88] appears at strong confinement.

4.1.1 Scaling regimes

The conditions and scaling predictions of regimes Ia-c and IIa-b are derived in Paper [I]. The derivations are based on the mean-field theory described in the previous chapter. In this section we reproduce the derivation of one regime (Ia) in some detail, and briefly discuss the other regimes. The result of this analysis is summarised in Tables 4.1–4.2 and Fig. 4.1. Table 4.1 and Fig. 4.1 shows the conditions that must be satisfied by D_H and D_W in order for the different regimes to apply. Table 4.2 shows the predicted scalings for the average and variance of the extension, along with references to the publications where these predictions were first derived. Table 4.2 also includes predictions for the free energy of confinement, which determines the work necessary to insert a polymer into a channel. In cases where exact predictions are known, they have been included in the table.

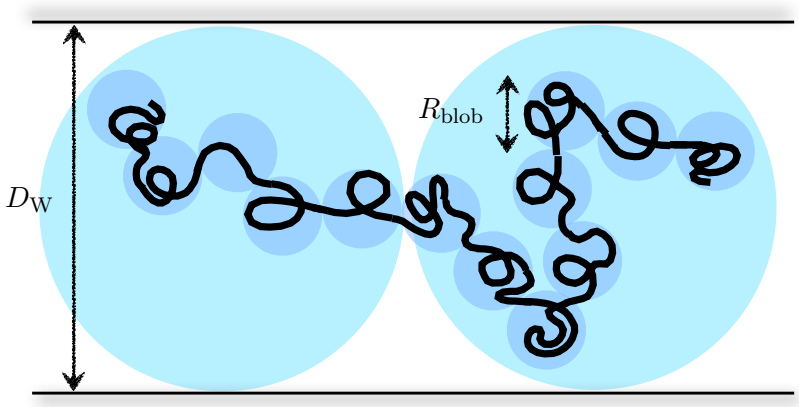

Figure 4.2: An illustration of the hierarchy of blobs analysed in regime I. In regime Ia, the smaller blobs are spherical blobs of size $R_{\text{blob}} = D_{\text{H}}$. In regime Ib-c they are cylindrical, of height D_{H} and width $R_{\text{blob}} > D_{\text{H}}$.

Regime Ia

Regime Ia is defined by the length scale relation

$$\ell_{\text{K}} \ll l_{\text{cc}} \ll l_{\text{ch}} \ll l_{\text{cw}} \ll L\,. \tag{4.1}$$

Since $l_{\text{cc}} \ll l_{\text{ch}}$, the polymer exhibits three-dimensional Flory scaling [Eq. (3.9)] before its first collision with the channel walls. The first collision with the ceiling or the floor must occur when a section of contour length l_{ch} has formed a spherical Flory blob of diameter D_{H}. According to Eq. (3.9), this occurs when

$$D_{\text{H}} \approx \left(l_{\text{ch}}^3 \ell_{\text{K}} w_{\text{eff}}\right)^{\frac{1}{5}} \Leftrightarrow l_{\text{ch}} \approx [D_{\text{H}}^5/(\ell_{\text{K}} w_{\text{eff}})]^{1/3}\,. \tag{4.2}$$

Consider now two neighbouring polymer segments, each of contour length l_{ch}. Each segment can be assumed to form a blob of approximate diameter D_{H}. Any significant overlap between the two blobs would result in a significant probability of overlaps between some of the polymer segments constituting the two blobs. Instead they line up next to each other. Similarly, N_{blobs} such segments form a string of N_{blobs} blobs, which performs a two-dimensional self-avoiding walk. This random walk of blobs must obey two-dimensional Flory scaling until the blobs have

formed a circular 'superblob' of diameter $D_{\rm W}$ (we follow the terminology of Ref. [89]). This two-dimensional random walk is illustrated in Fig. 4.2. The number of small spherical blobs constituting one superblob can be estimated from Eq. (3.17) with $\ell_{\rm K} = D_{\rm H}$ since each small spherical blob constitutes an independent segment of the walk. The assumption that the small blobs cannot overlap means that the two-dimensional excluded area of a blob approximately equals the area of a circle of diameter $D_{\rm H}$, in other words $a \approx D_{\rm H}^2$. This results in

$$D_{\rm W} \approx \left(N_{\rm blobs}^3 D_{\rm H}^4\right)^{\frac{1}{4}} \Leftrightarrow N_{\rm blobs} \approx (D_{\rm W}/D_{\rm H})^{4/3}\,. \tag{4.3}$$

The contour length stored within a superblob equals $l_{\rm cw}$,

$$l_{\rm cw} \approx N_{\rm blobs} l_{\rm ch} \approx [D_{\rm W}^4 D_{\rm H}/(\ell_{\rm K} w)]^{1/3}. \tag{4.4}$$

There are $L/l_{\rm cw}$ superblobs that line up along the channel [Fig. 4.2]. Each superblob has average diameter $D_{\rm W}$ with fluctuations of the same order (see section 3.2.2). The average extension and its fluctuations are therefore given by:

$$R \approx (L/l_{\rm cw}) D_{\rm W} \approx L\,[\ell_{\rm K} w/(D_{\rm H} D_{\rm W})]^{1/3}\,, \tag{4.5}$$

$$\sigma_{\rm R}^2 \approx (L/l_{\rm cw}) D_{\rm W}^2 \approx L\left(\ell_{\rm K} w D_{\rm W}^2/D_{\rm H}\right)^{1/3}\,. \tag{4.6}$$

It remains to derive the conditions for $D_{\rm H}$ and $D_{\rm W}$ under which Eq. (4.1) defining the regime holds. The inequality $l_{\rm cc} \ll l_{\rm ch}$ requires that ideal scaling within a blob of size $D_{\rm H}$ results in a large number of intra-chain overlaps,

$$(D_{\rm H}/\ell_{\rm K})^4 v/D_{\rm H}^3 \approx D_{\rm H} w/\ell_{\rm K}^2 \gg 1 \Leftrightarrow D_{\rm H} \gg \ell_{\rm K}^2/w. \tag{4.7}$$

The inequality $l_{\rm cw} \gg l_{\rm ch}$ is satisfied when $D_{\rm W} \gg D_{\rm H}$. Yet it turns out that in the limit $D_{\rm W} \to D_{\rm H}$ Eqs. (4.5)–(4.6) reproduce known results for square channels (see Section 4.1.3). This condition can therefore be relaxed.

Regime Ib

Just as in Regime Ia, the analysis in Regime Ib proceeds in terms of a hierarchy of blobs, as illustrated in Fig. 4.2. Yet the relation $l_{\rm ch} \ll l_{\rm cc}$ means that two blobs of size $D_{\rm H}$ are too dilute to be non-overlapping.

Instead ideal scaling will persist until cylindrical blobs have formed, of height D_H and diameter $R_\mathrm{blob} = \sqrt{l_\mathrm{cc}\ell_\mathrm{K}}$, where $l_\mathrm{cc} = \ell_\mathrm{K} D_\mathrm{H}/w_\mathrm{eff}$ [I]. From this point, the derivation is similar to that in Regime Ia, and yields identical scaling predictions for the mean and variance of the extension.

Regime IIa

Regime IIa is also called the extended de Gennes regime, and is discussed in detail in Paper [II], see Section 4.2. In this regime, the polymer obeys ideal scaling until a blob forms that fills the channel cross-section, and is further elongated along the channel direction, until it reaches an extension $R_\mathrm{blob} \approx \sqrt{l_\mathrm{cc}\ell_\mathrm{K}}$. From ideal scaling it follows that $l_\mathrm{ch} \approx D_\mathrm{H}^2/\ell_\mathrm{K}$, and $l_\mathrm{cw} \approx D_\mathrm{W}^2/\ell_\mathrm{K}$. The length scale l_cc is given by $l_\mathrm{cc} \approx \left(\frac{\ell_\mathrm{K} D_\mathrm{H}^2 D_\mathrm{W}^2}{w^2}\right)^{1/3}$ [I]. The polymer arranges itself into a line of L/l_cc blobs of size R_blob:

$$R \approx (L/l_\mathrm{cc}) R_\mathrm{blob} \approx L\,[\ell_\mathrm{K} w/(D_\mathrm{H} D_\mathrm{W})]^{1/3}, \tag{4.8}$$

$$\sigma_R^2 \approx (L/l_\mathrm{cc}) R_\mathrm{blob}^2 \approx L\ell_\mathrm{K}. \tag{4.9}$$

It is interesting to note that the scalings in regime IIa can be derived directly from a similar mean-field argument as in Section 3.2.1. The counterpart of Eq. (3.8) for the channel-confined polymer reads

$$\log P(r) \approx \text{const.} - \frac{r^2}{L\ell_\mathrm{K}} - \frac{L^2 w_\mathrm{eff}}{r D_\mathrm{W} D_\mathrm{H}}. \tag{4.10}$$

From this expression for the probability distribution of the extension Eqs. (4.8)–(4.9) follow. In Paper [III] we make use of Eq. (4.10) to derive approximate expressions for the extension statistics of a circular polymer (see Section 5.2).

Regimes Ic and IIb

The derivation in regime Ic (IIb) is very similar to the one in regime Ib (IIa), and leads to identical scaling predictions for the extension statistics. Note however that the prefactors are expected to differ between the regimes.

Regime III

Since the derivations in Regimes I and II are based on the mean-field theory discussed in the previous chapter, they apply not only to the

self-avoiding wormlike chain but to a large class of polymer models as discussed in section 3.2.1. By contrast, the predictions for Regime III are specific to the self-avoiding wormlike chain, and cannot be readily generalised to other models.

Regime IIIa

If $D_\mathrm{H} \leq D_\mathrm{W} \ll \ell_\mathrm{P}$ then the polymer is always almost perfectly aligned with the channel, only undulating slightly from side to side. This regime was first described in Ref. [90] and is usually referred to as the Odijk regime. Precise predictions for the mean and variance of the extension in the Odijk regime have been derived by Burkhardt et al. [87]:

$$R = L\left[1 - \alpha\frac{D_\mathrm{H}^{2/3} + D_\mathrm{W}^{2/3}}{\ell_\mathrm{P}^{2/3}}\right], \tag{4.11}$$

$$\sigma_R^2 = \beta L\frac{D_\mathrm{H}^2 + D_\mathrm{W}^2}{\ell_\mathrm{P}}. \tag{4.12}$$

Here $\alpha = 0.09137 \pm 0.00007$, $\beta = 0.00478 \pm 0.00010$ [87]. Note that in these formulas D_H and D_W refer to the size of the region that is accessible by the centre-line of the wormlike chain.

Regime IIIb

Odijk [86] has predicted the existence of a regime intermediate between the Odijk regime and the extended de Gennes regime, for very slender semi-flexible polymers. For square channels this regime was studied by Muralidhar *et al.* [83], who gave it the name "backfolded Odijk regime". In this regime the size of the channel is such that backfolds are possible but rare. Odijk defines the *global persistence length* g as the orientational correlation length of the corresponding ideal polymer. For an unconfined wormlike chain $g = \ell_\mathrm{P}$ [see Eq. (3.2)], yet at strong confinement the correlation length increases very significantly [84]. The backfolded Odijk regime requires that $\ell_\mathrm{P} \ll g \ll l_\mathrm{cc} \ll L$. Assuming that a polymer section that is free of backfolds follows the statistics of the Odijk regime, one can predict scaling relations for the extension in terms of the global persistence length g. However, no theory for how g itself depends on the channel size exists for relevant channel sizes [83]. Therefore we do not know where to draw the curve separating

Regimes IIIa and IIIb in Fig. 4.1. Simulations [83] indicate that the regime is virtually non-existent for DNA, manifesting itself clearly only for very slender polymers, i.e. polymers where the ratio $w_{\text{eff}}/\ell_{\text{P}}$ is very small.

4.1.2 Accuracy of mean-field theory

As discussed in section 3.2.2, the mean field predictions for the extension statistics are believed to be exact in two dimensions but only approximate in three dimensions. Using the improved scaling prediction of Eq. (3.16) would lead to modified scaling predictions for regime Ia: $R \approx LD_{\text{H}}^{-0.37}D_{\text{W}}^{-1/3}\ell_{\text{K}}^{0.40}w_{\text{eff}}^{0.30}$, $\sigma_R^2 \approx LD_{\text{H}}^{-0.37}D_{\text{W}}^{2/3}\ell_{\text{K}}^{0.40}w_{\text{eff}}^{0.30}$, $F_{\text{c}}/(k_{\text{B}}T) \approx LD_{\text{H}}^{-1.70}\ell_{\text{K}}^{0.40}w_{\text{eff}}^{0.30}$. The predictions in other regimes are not affected by this modification.

Apart from the use of mean-field arguments, the derivations in regimes I and II assume that the polymer can be divided into non-overlapping blobs. This argument is not rigorous. However, in regimes IIa-b it is possible to show that the scaling predictions are in fact exactly correct. In regime IIa it is further possible to derive rigorous bounds for the prefactors of the scaling laws. This derivation is discussed in paper [II] and section 4.2.

4.1.3 Reduction to known special cases

Square channels

For the special case $D_{\text{W}} = D_{\text{H}} = D$ the predictions of Paper [I] reproduce previous results for the special case of confinement in square channels. Thus the predictions of Regime Ia reproduce the known scalings of the de Gennes regime [82, 86], valid for $D \gg \ell_{\text{K}}^2/w_{\text{eff}}$. Regime IIa is a generalisation of the so called extended de Gennes regime [II, 80, 82, 85], valid when $\ell_{\text{K}} \ll D \ll \ell_{\text{K}}^2/w_{\text{eff}}$. This regime is discussed in detail in section 4.2.

Flexible polymers

For the special case of flexible polymers, for which $v \approx \ell_{\text{K}}^3$ and $l_{\text{cc}} \approx \ell_{\text{K}}$, only one scaling regime exists. The predictions of this regime are special cases of the predictions of regime Ia, in the case $\ell_{\text{K}} \approx w_{\text{eff}}$. The scaling

for the mean extension in this regime has previously been derived by Turban [89], using similar arguments as those employed here.

4.2 Exact results in the extended de Gennes regime

Blob and mean-field theories of the kind we employ in Paper [I] have been in use for a long time within polymer theory [68], and often yield results which are surprisingly accurate considering the simplicity of the arguments. However, they are not rigorous. Therefore it is difficult to predict their accuracy in circumstances where they have not been tested by other means, e.g. by simulations. Further, while they often predict the scaling behaviour of the average extension to a relatively high accuracy, they are often difficult to extend to higher orders and different observables. Finally, the obtained expressions are only ever valid up to an unknown prefactor, which both limits the predictive value of a theory and makes it more difficult to test.

In Paper [II] we develop a rigorous theory which improves upon the blob theory with regards to all the aspects listed above. Thus, the theory furnishes rigorous, quantitative predictions for the statistics of the extension and the end-to-end distance, and demonstrates the existence of a universal scaling law which applies also to other observables of the polymer confined in a channel. The theory applies in the extended de Gennes regime (regime IIa in tables 4.1–4.2 and Fig. 4.1), which is the relevant regime for many of the channel sizes that are used in DNA experiments [2].

4.2.1 Mapping to 1D model

To simplify the discussion, assume that the polymer is confined to a square channel of side length $D = D_{\mathrm{H}} = D_{\mathrm{W}}$. In this case the extended de Gennes regime is delimited by the conditions

$$\ell_{\mathrm{K}} \ll D \ll \ell_{\mathrm{K}}^2/w_{\mathrm{eff}}. \tag{4.13}$$

Further, because of the equivalence between polymer models (see Section 3.2.2), we can restrict the discussion to the special case of a freely jointed chain, consisting of N *monomers* with step length ℓ_{K}, with self-avoiding interactions such that two monomers cannot approach closer than a distance a. The model is illustrated in Fig. 4.3.

Table 4.1: Conditions for the scaling regimes of a semi-flexible polymer confined to a rectangular channel (adapted from the supplemental material of Paper [I]).

		Conditions		
Regime	Definition	D_H	D_W [a]	L
Ia	$\ell_\mathrm{K} \ll l_\mathrm{cc} \ll l_\mathrm{ch} \leq l_\mathrm{cw} \ll L$	$\gg \ell_\mathrm{K}^2/w_\mathrm{eff}$	—	$\gg \left(\frac{D_\mathrm{W}^4 D_\mathrm{H}}{\ell_\mathrm{K} w_\mathrm{eff}}\right)^{\frac{1}{3}}$
Ib	$\ell_\mathrm{K} \ll l_\mathrm{ch} \ll l_\mathrm{cc} \ll l_\mathrm{cw} \ll L$	$\ell_\mathrm{K} \ll D_\mathrm{H} \ll \ell_\mathrm{K}^2/w_\mathrm{eff}$	$D_\mathrm{W}^2 \gg D_\mathrm{H}\ell_\mathrm{K}^2/w_\mathrm{eff}$	$\gg \left(\frac{D_\mathrm{W}^4 D_\mathrm{H}}{\ell_\mathrm{K} w_\mathrm{eff}}\right)^{\frac{1}{3}}$
Ic	$l_\mathrm{ch} \ll \ell_\mathrm{K} \ll l_\mathrm{cc} \ll l_\mathrm{cw} \ll L$	$w_\mathrm{eff} \leq D_\mathrm{H} \ll \ell_\mathrm{K}$ [b]	$D_\mathrm{W}^2 \gg D_\mathrm{H}\ell_\mathrm{K}^2/w_\mathrm{eff}$	$\gg \left(\frac{D_\mathrm{W}^4 D_\mathrm{H}}{\ell_\mathrm{K} w_\mathrm{eff}}\right)^{\frac{1}{3}}$
IIa	$\ell_\mathrm{K} \ll l_\mathrm{ch} \leq l_\mathrm{cw} \ll l_\mathrm{cc} \ll L$	$\ell_\mathrm{K} \ll D_\mathrm{H} \ll \ell_\mathrm{K}^2/w_\mathrm{eff}$	$D_\mathrm{W}^2 \ll D_\mathrm{H}\ell_\mathrm{K}^2/w_\mathrm{eff}$	$\gg \left(\frac{D_\mathrm{H}^2 D_\mathrm{W}^2 \ell_\mathrm{K}}{w_\mathrm{eff}^2}\right)^{\frac{1}{3}}$
IIb	$l_\mathrm{ch} \ll \ell_\mathrm{K} \ll l_\mathrm{cw} \ll l_\mathrm{cc} \ll L$	$w_\mathrm{eff} \ll D_\mathrm{H} \ll \ell_\mathrm{K}$	$\ell_\mathrm{K}^2 \ll D_\mathrm{W}^2 \ll \frac{D_\mathrm{H}\ell_\mathrm{K}^2}{w_\mathrm{eff}}$	$\gg \left(\frac{D_\mathrm{H}^2 D_\mathrm{W}^2 \ell_\mathrm{K}}{w_\mathrm{eff}^2}\right)^{\frac{1}{3}}$
IIIa	$l_\mathrm{ch} \leq l_\mathrm{cw} \ll \ell_\mathrm{P}$, $l_\mathrm{cw} \ll L$ [c]	$D_\mathrm{H} \ll \ell_\mathrm{P}$	$D_\mathrm{W} \ll \ell_\mathrm{P}$	$\gg \ell_\mathrm{P}^{\frac{1}{3}} D_\mathrm{W}^{\frac{2}{3}}$
IIIb	$l_\mathrm{ch} \leq l_\mathrm{cw} \leq \ell_\mathrm{P} \ll g \ll l_\mathrm{cc} \ll L$ [d]	$D_\mathrm{H} \leq D_\mathrm{W} \lesssim \ell_\mathrm{P}$, $\frac{g w_\mathrm{eff}}{\ell_\mathrm{P}^{\frac{1}{3}} D_\mathrm{W}^{\frac{2}{3}} D_\mathrm{H}} \ll 1$		$\gg \left(\frac{g^{\frac{1}{2}} \ell_\mathrm{P}^{\frac{1}{3}} D_\mathrm{H} D_\mathrm{W}^{\frac{2}{3}}}{w_\mathrm{eff}}\right)^{\frac{2}{3}}$

[a] It is assumed throughout that $D_\mathrm{W} \geq D_\mathrm{H}$.

[b] Tree et al. [92] have shown in simulations that for polymers confined in slits, the non-crossing regime $D_\mathrm{H} < w_\mathrm{eff}$ is approached smoothly as $D_\mathrm{H} \to w_\mathrm{eff}$ from above, and we expect the same to be valid in channels.

[c] Whereas conditions and predictions involving ℓ_P are specific to the wormlike chain, those expressed in terms of ℓ_K are valid for general polymer models, if the effective width w_eff is replaced by v/ℓ_K^2, where v is the excluded volume of a Kuhn length segment.

[d] The global persistence length g is the orientational correlation length of the confined polymer, defined in Refs. [83, 86].

Table 4.2: Predictions for the scaling regimes of a semi-flexible polymer confined to a rectangular channel (adapted from the supplemental material of Paper [I]).

Regime	R/L	σ_R^2/L	$F_c/(k_BTL)$
Ia	$\approx \left(\frac{\ell_K w_{eff}}{D_H D_W}\right)^{\frac{1}{3}}$ [93]	$\approx \left(\frac{\ell_K w_{eff} D_W^2}{D_H}\right)^{\frac{1}{3}}$ [I]	$\approx \left(\frac{\ell_K w_{eff}}{D_H^5}\right)^{\frac{1}{3}}$ [I]
Ib	$\approx \left(\frac{\ell_K w_{eff}}{D_H D_W}\right)^{\frac{1}{3}}$ [I]	$\approx \left(\frac{\ell_K w_{eff} D_W^2}{D_H}\right)^{\frac{1}{3}}$ [I]	$= \frac{\pi^2}{6}\ell_K D_H^{-2}$ [94][a]
Ic	$\approx \left(\frac{\ell_K w_{eff}}{D_H D_W}\right)^{\frac{1}{3}}$ [I]	$\approx \left(\frac{\ell_K w_{eff} D_W^2}{D_H}\right)^{\frac{1}{3}}$ [I]	$= 1.1032(1)\ell_P^{-\frac{1}{3}} D_H^{-\frac{2}{3}}$ [91]
IIa	$= 0.9338(84)\left(\frac{\ell_K w_{eff}}{D_H D_W}\right)^{\frac{1}{3}}$ [II]	$= 0.13(1)\ell_K$ [II]	$= \frac{\pi^2}{6}\ell_K(D_H^{-2} + D_W^{-2})$ [94]
IIb	$\approx \left(\frac{\ell_K w_{eff}}{D_H D_W}\right)^{\frac{1}{3}}$ [86]	$= 0.20(2)\ell_K$ [II][b]	$= 1.1032(1)\ell_P^{-\frac{1}{3}} D_H^{-\frac{2}{3}}$ [91]
IIIa	$= 1 - 0.09137(7)\frac{D_H^{\frac{2}{3}} + D_W^{\frac{2}{3}}}{\ell_P^{\frac{2}{3}}}$ [87]	$= 0.00478(10)\frac{D_H^2 + D_W^2}{\ell_P}$ [87]	$= 1.1032(1)\ell_P^{-\frac{1}{3}}(D_H^{-\frac{2}{3}} + D_W^{-\frac{2}{3}})$ [91]
IIIb	$\approx \left(\frac{g w_{eff}}{\ell_P^{\frac{1}{3}} D_W^{\frac{2}{3}} D_H}\right)^{\frac{1}{3}}$ [86]	$\approx g$ [83]	$\approx \ell_P^{-\frac{1}{3}} D_H^{-\frac{2}{3}}$ [83]

[a] Exact predictions are asymptotically valid in the limit when the parameter conditions are extremely well satisfied. In some cases, higher order corrections are known.

[b] The step variance σ_0^2 [II] obeys $\sigma_0^2 = \ell_K^2/2$ in this regime.

We proceed to show that in the extended de Gennes regime it is possible to map the extension statistics to a one-dimensional random walk model. For this model, a number of results have been derived, and we discuss the implications for the statistics of the confined polymer.

As described in section 3.2.1, one way to obtain a statistically correct ensemble for the self-avoiding polymer is to start from an ensemble of the corresponding ideal polymer, and then discard any configurations involving overlaps. The z-coordinates of the ideal polymer obey the statistics of a one-dimensional random walk with independent steps of mean 0 and variance $\sigma_0^2 = \ell_K^2/3$. Denote the probability distribution of a certain set of z-coordinates for the ideal chain by $P_{\text{ideal}}(\{z_n\})$. Here z denotes the direction parallel to the channel axis. The corresponding distribution for the self-avoiding chain is then given by

$$P(\{z_n\}) \propto P_{\text{ideal}}(\{z_n\})A(\{z_n\})\,. \tag{4.14}$$

Note the similarity with Eq. (3.6) for the unconfined chain. As in that equation, the acceptance function $A(\{z_n\})$ denotes the fraction of ideal configurations that are free of overlaps.

Consider now two monomers m and n. Obviously they can only overlap if their z-coordinates are sufficiently close, namely if $|z_n - z_m| < a$ (recall that a is the diameter of a bead). If this condition is satisfied, what is then the overlap probability? In general this is a difficult question to answer, as the probability depends not only on the separation $|n - m|$, but also on the z-coordinates of intermediate monomers. However, if the contour separation is much larger than the length scale l_{cw} between collisions with the channel walls, then the probability is simply a constant number (which we compute below). This follows from the fact that at large separations the x- and y-coordinates of two monomers are statistically independent [II, B].

The condition $l_{\text{cw}} \ll l_{\text{cc}}$ defining the extended de Gennes regime implies that almost all overlaps occur between monomers at such a large separation. The acceptance function $A(\{z_n\})$ therefore acquires a simple form, which allows us to map the statistics to a one-dimensional random walk model, as follows: Imagine dividing the z-axis into bins of size ϵ, where $a \ll \epsilon \ll \ell_K$ [see Fig. 4.3(c)]. For two monomers to collide, their z-coordinates must lie in the same bin, i.e. $\lfloor z_n/\epsilon \rfloor = \lfloor z_m/\epsilon \rfloor$, where $\lfloor x \rfloor$ is the floor function. Supposing that they do, we write the probability for the monomers to collide as $2\eta/\epsilon$, the constant of proportionality

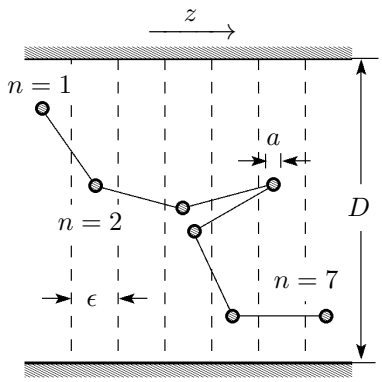

Figure 4.3: An illustration of the freely-jointed-chain model and the principle behind the mapping to a one-dimensional model.

η is discussed below. Assuming that $\eta/\epsilon \ll 1$ the factor $A(\{z_n\})$ in Eq. (4.14) can be written as

$$A(\{z_n\}) = \prod_{\substack{1\le n<m\le N \\ \lfloor z_n/\epsilon\rfloor=\lfloor z_m/\epsilon\rfloor}} (1-2\eta/\epsilon) = \exp\left[-\frac{2\eta}{\epsilon}\sum_{1\le n<m\le N}\delta^{(\epsilon)}_{z_n,z_m}\right]. \tag{4.15}$$

Here $\delta^{(\epsilon)}_{z_n,z_m}$ is unity if z_n and z_m fall into the same bin, and zero otherwise.

The problem of describing the conformations of the confined polymer is thus mapped to that of a random walk on $\mathbb{Z}$, consisting of N steps with variance σ_0^2/ϵ^2. Each time two steps land on the same integer, the walk incurs a 'penalty' of $2\eta/\epsilon$. This problem is known as the weakly self-avoiding random walk or the Domb-Joyce model in one dimension [95].

It remains to compute the constant of proportionality η. For any monomer not too close to either end of the polymer, the probability distribution of its x- and y-coordinates is given by [B, 68]

$$\rho(x,y) = (2/D)^2 \sin^2(\pi x/D)\sin^2(\pi y/D). \tag{4.16}$$

Consider now two monomers in the same bin of width ϵ. Assuming that the first monomer has coordinates x and y, then the probability that the second monomer overlaps with it is $v/\epsilon\rho(x,y)$, where v is the excluded volume of each monomer. Averaging this probability over the distribution $\rho(x,y)$ yields the probability $2\eta/\epsilon$, or

$$\eta = \frac{v}{2}\iint_0^D \mathrm{d}x\mathrm{d}y\,\rho^2(x,y) = \frac{9}{8}\frac{v}{D^2}. \tag{4.17}$$

4.2.2 Implications for the confined polymer

The mapping to a one-dimensional weakly self-avoiding random walk is significant because exact asymptotic solutions have been obtained for this model in the limit where η/σ_0 is small, as is always the case in the extended de Gennes regime. For the confined polymer the main implications are listed below.

1. A scaling relation holds for the one-dimensional weakly self-avoiding random walk [95]. For the confined polymer, this relation implies that expressing results in terms of the scaled variables

$$n' = n\,(\eta/\sigma_0)^{2/3} \quad \text{and} \quad z' = (z/\sigma_0)\,(\eta/\sigma_0)^{1/3} \tag{4.18}$$

   must give rise to universal laws.

2. The distribution of the extension $R_z = \max_i z_i - \min_i z_i$ of the polymer in the channel acquires a large-deviation form in the limit of large N [95],

$$P(R_z) \sim \exp[-NS(R_z/(N\sigma_0), \eta/\sigma_0)]\,. \tag{4.19}$$

   Eq. (4.18) implies that the 'action' S obeys the scaling law

$$S\Big(\frac{R_z}{N\sigma_0}, \frac{\eta}{\sigma_0}\Big) = \Big(\frac{\eta}{\sigma_0}\Big)^{2/3} J\Big[\Big(\frac{\eta}{\sigma_0}\Big)^{-1/3} \frac{R_z}{N\sigma_0}\Big]\,, \tag{4.20}$$

   where $J(b)$ is a scaling function.

3. The distribution $P(r_z)$ of the end-to-end distance $r_z = |z_1 - z_N|$ is also of the form (4.19,4.20) save for a different scaling function $I(b)$ that replaces $J(b)$ [96] The functions $I(b)$ and $J(b)$ are identical above a critical value $b^{**} = 0.85$ [97]. Since the only minimum of the function $J(b)$ lies above this critical value, the mean and variance of the end-to-end distance and the extension must agree for very long chains. Yet the small-b behaviour of I and J differ substantially. For $b < b^{**}$ $I(b)$ is linear in b, whereas $J(b)$ is strictly convex and rapidly increases with decreasing b [97].

4. The statistical properties of the extension and end-to-end distance can be determined from the shape of the function $J(b)$ [or $I(b)$]. The location b^* of the minimum of J gives the mean R of R_z, and

the curvature $1/c^{*2}$ at this point yields the corresponding variance σ_R^2:

$$R/N = b^* \sigma_0^{2/3} \eta^{1/3}\,, \tag{4.21}$$

$$\sigma_R/\sqrt{N} = c^* \sigma_0\,. \tag{4.22}$$

Rigorous bounds for the universal parameters b^* and c^* were obtained in Refs. [95, 98]: $1.104 \leq b^* \leq 1.124$, and $0.60 \leq c^* \leq 0.66$. Applied to the self-avoiding wormlike chain, Eqs. (4.21)–(4.22) yield the predictions

$$R = 0.9338(84) L \left(\frac{\ell_{\mathrm{K}} w_{\mathrm{eff}}}{D^2} \right)^{1/3}\,, \tag{4.23}$$

$$\sigma_R^2 = 0.13(1) L \ell_{\mathrm{K}}\,. \tag{4.24}$$

4.2.3 Comparison to simulations

To verify the above predictions, we have performed Monte Carlo simulations of the freely-jointed chain model. These simulations were performed in relatively small channels, for which Eq. (4.16) only holds approximately. In order to nevertheless obtain a good estimate for η we used a numerical solution for the equilibrium distribution $\rho(x, y)$ of a monomer in the ideal freely jointed chain[1].

[1] $\rho(x, y)$ was computed as follows: Let $G_N(\mathbf{r})$ be proportional to the probability density of finding the final monomer N at $\mathbf{r}$. G_N obeys the equation

$$G_n(\mathbf{r}) = \int d\mathbf{r}' G_{n-1}(\mathbf{r}') G_1(\mathbf{r} - \mathbf{r}'), \tag{4.25}$$

where $G_1(\mathbf{r} - \mathbf{r}') \equiv 1/(4\pi\ell_{\mathrm{K}}^2)\delta(|\mathbf{r} - \mathbf{r}'| - \ell_{\mathrm{K}})$ is the probability distribution of one bond vector. For the channel-confined polymer, the equation must be supplemented by absorbing boundary conditions [99]: $G = 0$ outside of the channel. We now make the approximation that G_n factorises, i.e. that $G_n(\mathbf{r}) = G_n^{\perp}(x) G_n^{\perp}(y) G_n^{\parallel}(z)$. Then, the equation for $G_n^{\perp}(x)$ is simply

$$G_n^{\perp}(x) = (2\ell_{\mathrm{K}})^{-1} \int_{-\ell_{\mathrm{K}}}^{\ell_{\mathrm{K}}} \mathrm{d}\delta x\, G_{n-1}^{\perp}(x - \delta x), \tag{4.26}$$

with initial condition $G_0^{\perp}(x) = 1/D$ and boundary conditions $G_n^{\perp}(x) = 0$ unless $0 < x < D$. This equation was discretised and solved by iterating the above equation until it converged (up to a normalising factor). Call the resulting function $G(x)$. The distribution $\rho(x, y)$ of a monomer far from either end of the chain is given by $\rho(x, y) \propto [G(x)G(y)]^2$ [B].

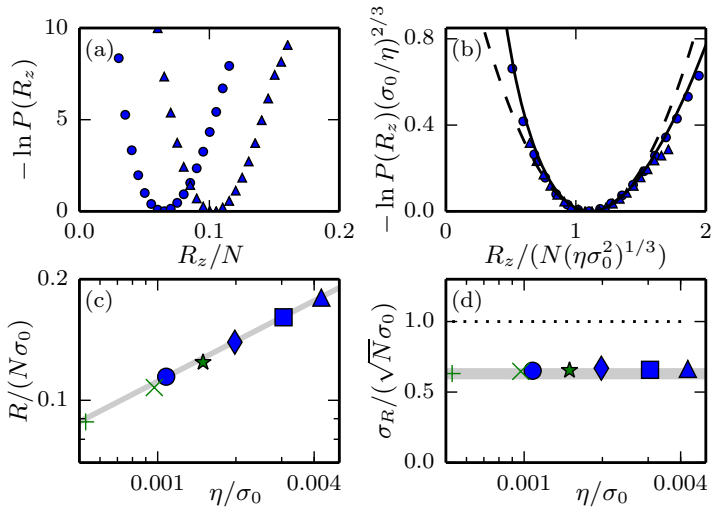

Figure 4.4: (a) Distribution $P(R_z)$ of the extension R_z for $D/\ell_K = 4, a/\ell_K = 0.14$ (○), $a/\ell_K = 0.22$ (△). (b) Same distributions plotted as a function of the scaled variable $R_z/[N(\eta\sigma_0^2)^{1/3}]$, Eqs. (4.19) and (4.20). Also shown is the asymptotic exact solution $J(b)$ (solid line, see text) as well as a Gaussian approximation (dashed line). (c) Scaling prediction for the mean extension [Eq. (4.21)], shaded grey area. Its width corresponds to the uncertainty of the coefficient b^* given in the text below Eq. (4.22). Also shown are results of Monte-Carlo simulations (symbols) for $D/\ell_K = 4$, $a/\ell_K = 0.14$ (○), 0.17 (◊), 0.20 (□), 0.22 (△) and $D/\ell_K = 6$, $a/\ell_K = 0.14$ (+), 0.17 (×), 0.20 (∗). (d) Standard deviation of the extension distribution from simulations (symbols), compared to Eq. (4.22), shaded grey area. The dotted line indicates the variance of the corresponding ideal polymer.

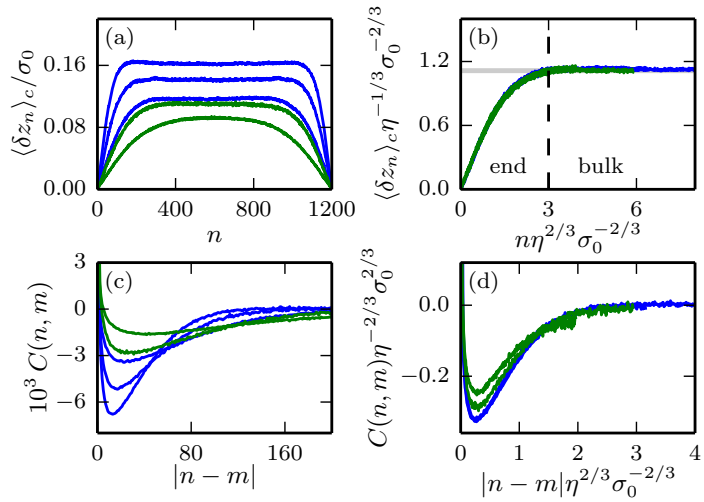

Figure 4.5: (a) Bias (see text) as a function of monomer number. (b) Data in the left half of panel a, rescaled to show the universality of the shape. Shaded grey area: prediction from Eq. (4.21). The vertical dashed line indicates the boundary between the end and the bulk regions of the polymer globule. (c) The correlation function $C(n, m)$ (defined in the text) averaged over n, m in the interior of the polymer (the plateau of panel a). (d) The rescaled correlation function, showing the universal 'correlation hole'. In both panels, blue (green) lines correspond to $D = 4\ell_K$ ($D = 6\ell_K$). In order of increasing η, the monomer diameter is given by $a/\ell_K = 0.14, 0.17$ (green); $0.14, 0.17, 0.20$ (blue).

The results from simulations are shown in Figs. 4.4–4.5. Fig. 4.4 shows that the distribution of the extension obeys Eqs. (4.20)–(4.22), whereas Fig. 4.5 shows that the universal scaling of Eq. (4.18) holds also for local observables.

Fig. 4.4(a) plots the distribution of R_z for two different sets of parameters. Panel (b) shows that the data collapse upon scaling the x- and y-axes according to (4.20). We computed the universal scaling function, $J(b)$, by numerical solution of an eigenvalue problem (Eq. (3.49) in Ref. [100] and Eq. (0.15) in Ref. [101]). The result is plotted in Fig. 4.4(b) as a solid line. We observe excellent agreement far into the non-Gaussian tails of the distribution. Panels (c) and (d) show that the mean and variance of the extension are in agreement with Eqs. (4.21)–(4.22).

Fig. 4.5 (a) shows the bias $\langle \delta z_n \rangle_c \equiv \langle \delta z_n \, \mathrm{sgn}(z_N - z_1) \rangle$ (where $\mathrm{sgn}(x)$ is the signum function), which quantifies the tendency of all steps of the corresponding random walk to point in the same direction. Panel (b) demonstrates that all data points collapse to a universal curve when rescaled according to Eq. (4.18). Far from either end the bias must approach the bulk prediction (4.21). Fig. 4.5(b) shows that this is indeed the case. Near the end of the polymer the bias is smaller. This end effect gives rise to finite-size corrections for the end-to-end distance.

Panel (c) shows the correlation function of the steps,

$$C(n,m) = (\langle \delta z_n \delta z_m \rangle_c - \langle \delta z_n \rangle_c \langle \delta z_m \rangle_c)/\sigma_0^2. \tag{4.27}$$

Panel (d) shows the rescaled version. Since $\sigma_{r_z}^2 = \sigma_0^2 \sum_{n,m=1}^{N} C(n,m)$, the fact that the steps are negatively correlated is related to the fact that the fluctuations of r_z are smaller than those of an ideal polymer.

Summary

In Paper [I] we demarcate the scaling regimes of a semiflexible polymer confined to a rectangular channel. We find that the extension statistics depend not only on the area of the channel cross-section, but also on its shape. For this reason rectangular channels exhibit features which are absent in the commonly studied special case of square channels.

In Paper [II] we show that in the experimentally relevant extended de Gennes regime the statistics of a confined polymer can be mapped rigorously to a one-dimensional model. From this mapping follows not

only a rigorous proof of the mean-field scaling for the extension statistics and its associated prefactors, but also the existence of a universal scaling law. The scaling law implies that any results that have been derived for one set of parameters (e.g. by simulations of either the 3D or the 1D model) can be directly translated to any other set of parameters within the extended de Gennes regime.

Chapter 5. Comparison to experiment

This chapter describes the results of Refs. [III] and [IV]. These papers consist of experimental measurements of the extension statistics of channel-confined DNA, and comparisons to the theories described in Chapter 4. Paper [III] is summarised in Section 5.2. In this paper, we induce a confined circular DNA molecule to break, forming a linear molecule of equal contour length. The linear molecule spontaneously unfolds in the channel, allowing us both to study the dynamics of the unfolding process and to compare the equilibrium statistics of the polymer in the circular and linear state. Since I mainly contributed to the latter part of the study, this is the focus of Section 5.2.

Paper [IV] is summarised in Section 5.3. Here we measure the extension statistics of linear DNA molecules under conditions which satisfy the conditions of the extended de Gennes regime to varying degrees. These measurements are compared to the predictions of Paper [II]. Since a quantitative fit between experiment and theory requires that the parameters L, ℓ_{K} and w_{eff} are known to a high degree of accuracy, this comparison affords a test not only of the predictions of paper [II], but also of the theories for the physical parameters that characterise DNA, described in Chapter 2.

5.1 Brief summary of the experimental method

In the experiments described in this chapter, DNA molecules are inserted into nanochannels and imaged by epifluorescence microscopy. Channels are etched out of silicon dioxide, and DNA molecules are inserted using pressure-driven flow.

DNA samples are immersed in TBE buffer at different concentrations. 1×TBE contains 0.089 M Tris, 0.089 M Borate and 0.0020 M EDTA. The antioxidant β-mercaptoethanol (BME) is added to reduce photon-induced breaking of the DNA molecules, at a concentration of 3 μL of BME to 97 μL of sample solution. In order to fluoresce, DNA molecules are stained with the dye YOYO-1 (see Section 2.3).

The fluorescence of the stained DNA is recorded by an EMCCD camera, see Fig. 5.1(c) for snapshots from the resulting videos. In each image the DNA extension is given by the size of the fluorescing region. This results in a data series of DNA extension as a function of time,

from which we obtain the extension statistics.

Details about the experimental procedure are given in the respective papers [III, IV]. A more in-depth discussion of the experimental techniques can be found in the review articles [2, 5].

5.2 Unfolding circular DNA

In Paper [III] circular DNA is inserted into nanochannels of width $D_W \approx 100\,\text{nm}$ and depths of either $D_H \approx 100\,\text{nm}$ or $D_H \approx 150\,\text{nm}$. The DNA consists of 42200 base pairs. Assuming that the intercalation ratio is 1:10 (i.e. 1 bound dye molecule for each 10 base pairs), this corresponds to a contour length of approximately 16.2 µm (see Chapter 2).

DNA stained by a fluorescent dye such as YOYO-1 has a tendency to undergo photonicking, meaning that the excited dye causes one of the strands of the DNA molecule to break [102]. If two such nicks occur sufficiently close to each other, but on opposite strands, the molecule may break. If this happens on a linear DNA molecule, two shorter linear molecules are formed. By contrast, a break on a circular molecule changes the configuration into a linear molecule of the same length. The linear DNA then spontaneously unfolds to a more extended configuration. This allows one to study the dynamics of the unfolding process, and also to compare the equilibrium statistics of a linear polymer to that of its circular counterpart under essentially identical external conditions.

The unfolding process is shown in Fig. 5.1(a) by means of a 'kymograph'. It is constructed as follows: First, the part of the recording containing the confined polymer is identified, as in panel (c). Each frame of the video is then collapsed to a single horizontal line by averaging the brightness values over the direction perpendicular to the channel. A kymograph is formed by stacking the lines on top of each other, to show how the fluorescence pattern changes over time.

Figure 5.1(a) shows two examples of the unfolding process. In these kymographs, the bright region in the upper half of the picture corresponds to unbroken circular DNA fluctuating in the channel. After a while a breaking event occurs, either in the interior of the molecule (left column) or close to one of the ends (right column). The resulting linear molecule then unfolds. The unfolding can be observed as the simultaneous shrinking of the bright region (corresponding to folded DNA) and growing of a fainter region (unfolded DNA). After some time,

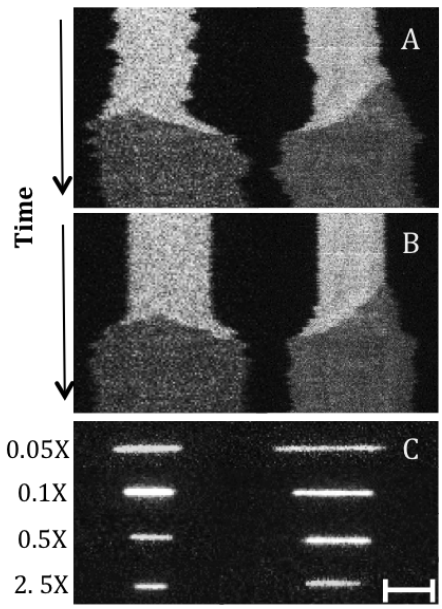

Figure 5.1: Kymographs, i.e. time (y-axis) vs. extension (x-axis), showing unfolding of circular DNA: (a) Raw kymographs, (b) Kymographs aligned by the centre of mass. Left: Circular DNA unfolding from the centre. Right: Circular DNA unfolding from the end. See text for an explanation of how to interpret these kymographs.
(c) Snapshots of YOYO-1–stained circular DNA before (left) and after (right) unfolding at four different buffer concentrations in channels with dimensions of about $150 \times 100\,\mathrm{nm}^2$ for 0.1×TBE, 0.5×TBE and 2.5×TBE solutions, and $100 \times 100\,\mathrm{nm}^2$ for 0.05×TBE. The scale-bar corresponds to 5 µm in all images.

the molecule is entirely unfolded, and we can observe the equilibrium fluctuations of the linear DNA.

We measure the mean and standard deviation of the extension in the circular (R_{circ}, σ_{circ}) and linear (R_{lin}, σ_{lin}) state, and test whether the ratios $R_{\mathrm{lin}}/R_{\mathrm{circ}}$ and $\sigma_{\mathrm{lin}}/\sigma_{\mathrm{circ}}$ are consistent with theoretical expectations. Since the channel size is intermediate between the Odijk regime (strong confinement, large extension) and the extended de Gennes regime (weaker confinement, smaller extension), it is difficult to make a quantitative comparison to theory. However, we show that the measured ratios are intermediate between our predictions for the Odijk regime and the extended de Gennes regime, with observations at stronger confinement yielding ratios closer to the prediction in the Odijk regime, and vice versa.

5.2.1 Theoretical predictions for the ratios $R_{\mathrm{lin}}/R_{\mathrm{circ}}$ and $\sigma_{\mathrm{lin}}/\sigma_{\mathrm{circ}}$

The extended de Gennes regime

In the extended de Gennes regime, the mapping to a one-dimensional model discussed in Chapter 4 yields exact predictions for the extension and variance of a linear polymer [Eqs. (4.23)–(4.24)]. Unfortunately corresponding expressions for circular polymers are not known. However, we know that the scalings (though not the prefactors) can also be derived directly from a mean-field argument (see Section 4.1.1). For the linear polymer, the probability distribution for the extension can be estimated by Eq. (4.10), which we rewrite as

$$\log P(R_{\mathrm{lin}}) = \text{const.} - A\frac{R_{\mathrm{lin}}^2}{L\ell_{\mathrm{K}}} - B\frac{L^2 w_{\mathrm{eff}}}{R_{\mathrm{lin}} D_{\mathrm{W}} D_{\mathrm{H}}}. \tag{5.1}$$

Here, A and B are prefactors of order unity which we have inserted to emphasise that the mean-field estimate does not determine the prefactors of the scaling. Eq. (5.1) yields an average extension and variance of

$$R_{\mathrm{lin}} = L\left(\frac{B\ell_{\mathrm{K}} w_{\mathrm{eff}}}{2AD_{\mathrm{W}}D_{\mathrm{H}}}\right)^{1/3}, \tag{5.2}$$

$$\sigma_{\mathrm{lin}}^2 = \frac{L\ell_{\mathrm{K}}}{6A}. \tag{5.3}$$

A similar mean-field estimate for the distribution of a circular polymer is obtained by treating the circular molecule as two linear polymers of

length $L/2$, which are forced to occupy the same part of the channel. This calculation results in

$$\log P(R_{\rm circ}) = \text{const.} - 2A\frac{R_{\rm lin}^2}{(L/2)\ell_{\rm K}} - B\frac{L^2 w_{\rm eff}}{R_{\rm lin}D_{\rm W}D_{\rm H}}. \tag{5.4}$$

$$R_{\rm circ} = L\left(\frac{B\ell_{\rm K}w_{\rm eff}}{8AD_{\rm W}D_{\rm H}}\right)^{1/3}, \tag{5.5}$$

$$\sigma_{\rm circ}^2 = \frac{L\ell_{\rm K}}{24A}. \tag{5.6}$$

Comparing Eqs. (5.2),(5.3) and Eqs. (5.5),(5.6) yields our prediction for the ratios in the extended de Gennes regime,

$$\frac{R_{\rm lin}}{R_{\rm circ}} = 2^{2/3} = 1.59. \tag{5.7}$$

$$\frac{\sigma_{\rm lin}}{\sigma_{\rm circ}} = 2. \tag{5.8}$$

The Odijk regime

In the Odijk regime the mean and variance of the extension for a linear DNA molecule confined to a rectangular channel $D_{\rm W} \times D_{\rm H}$ are given by Eqs. (4.11)–(4.12):

$$R_{\rm lin} = L\left[1 - \alpha\frac{D_{\rm W}^{2/3} + D_{\rm H}^{2/3}}{\ell_{\rm P}^{2/3}}\right], \tag{5.9}$$

$$\sigma_{\rm lin}^2 = \beta L\frac{D_{\rm W}^2 + D_{\rm H}^2}{\ell_{\rm P}}, \tag{5.10}$$

where $\alpha = 0.09137 \pm 0.00007$, $\beta = 0.00478 \pm 0.00010$ [87]. As in the extended de Gennes regime, a circular DNA in the Odijk regime can be treated as two linear DNA molecules occupying the same part of the channel. Calculating the statistics of the extension is complicated by the interaction between the two strands. Yet the extension can be bounded above and below by considering the two extreme cases of either no interaction, or complete separation such that each strand only explores half of the channel. For a square channel[1] this analysis yields that the

[1] In some of our experiments the channels are only approximately square ($D_{\rm H} = 100\,\text{nm}$, $D_{\rm W} = 150\,\text{nm}$).

mean and variance of the extension are bounded by

$$\frac{L}{2}\left[1-2\alpha\frac{D^{2/3}}{\ell_{\mathrm{P}}^{2/3}}\right] \leq R_{\mathrm{circ}} \leq \frac{L}{2}\left[1-1.63\alpha\frac{D^{2/3}}{\ell_{\mathrm{P}}^{2/3}}\right], \tag{5.11}$$

$$\beta L\frac{5D^2}{16\ell_{\mathrm{P}}} \leq \sigma^2 \leq \beta L\frac{D^2}{2\ell_{\mathrm{P}}}. \tag{5.12}$$

Here D is the side length of the square channel. Comparing Eqs. (5.9) and (5.11) yields a ratio of extensions in the interval

$$1.92 \leq R_{\mathrm{lin}}/R_{\mathrm{circ}} \leq 2. \tag{5.13}$$

As D tends to zero, the ratio tends to 2 regardless of how the strands interact. The lower bound comes from the assumption that the Odijk regime extends up to channel sizes of $D = \ell_{\mathrm{P}}$. Comparing instead Eqs. (5.10) and (5.12) shows that the ratio of standard deviations must lie in the interval

$$2 \leq \sigma_{\mathrm{lin}}/\sigma_{\mathrm{circ}} \leq 2.5. \tag{5.14}$$

5.2.2 Experimental results

Fig. 5.2 shows the experimental measurements of the equilibrium extension of each molecule, as a scatter plot of the linear extension over the circular extension. For both the linear and circular configuration, the extension is higher on average when the buffer concentration is low[2]. This is expected, as the effective width grows with decreasing ionic strength (see Table 2.1). The experimental data consistently falls between the predictions in the extended de Gennes regime [Eq. (5.7)] and the Odijk regime [Eq. (5.13)], with the data points at a larger extension agreeing better with the prediction in the Odijk regime and vice versa.

There is one problem with the interpretation of the data which is worth mentioning. A large part of the variation within each buffer condition is probably due to differences in the amount of dye bound to the DNA [103]. Yet the largest effect of YOYO-1 intercalation on the physical properties of DNA is probably that it increases the contour length (see Chapter 2). Since this effect is not considered when estimating the contour length it is probable that the the contour length

[2]At the lowest ionic strength (0.05×TBE) slightly smaller channels were used, further increasing the extension.

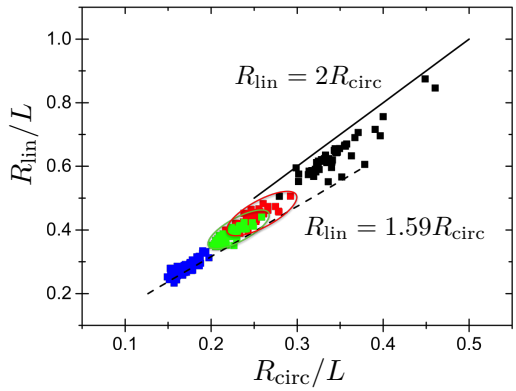

Figure 5.2: Equilibrium extension divided by contour length for circular (x-axis) and linear (y-axis) configurations of DNA. Each data point represents a single molecule confined to $150 \times 100\,\mathrm{nm}^2$ channels in 2.5×TBE (blue squares), 0.5×TBE (green squares), and 0.1×TBE (red squares). Black squares correspond to $100 \times 100\,\mathrm{nm}^2$ channels in 0.05×TBE. The red and green circles emphasise the overlap between the data points at 0.5× and 0.1×TBE. The dashed line shows the expected relation in the extended de Gennes regime [$R_{\rm lin} = 1.59R_{\rm circ}$, see Eq. (5.7)]. The solid line corresponds to the upper bound in the Odijk regime [$R_{\rm lin} = 2R_{\rm circ}$, see Eq. (5.13)].

is underestimated for the most extended molecules within each group. Note that as this does not influence the ratio $R_{\rm lin}/R_{\rm circ}$, it does not affect the conclusions of the paper.

Figure 5.3 shows equilibrium extension fluctuations for the circular and linear configuration of the same DNA molecule. Although the spread is much larger than for the extension ratio in Figure 5.2, there is a clear trend that the fluctuations decrease with decreasing buffer concentration. This is consistent with the theoretical prediction that fluctuations are smaller in the Odijk regime. For each condition the average ratio is slightly above 2, and increases as we move from the extended de Gennes regime (ratio = 2) towards the Odijk regime (ratio ≥ 2).

For very slender polymers, an additional regime known as the back-folded Odijk regime appears for channel sizes intermediate between the extended de Gennes regime and the Odijk regime [84, 86]. In this regime the fluctuations should increase as the ratio $D/\ell_{\rm P}$ decreases [84]. However, Fig. 11 of Ref. [84] shows that for DNA, this regime exists only

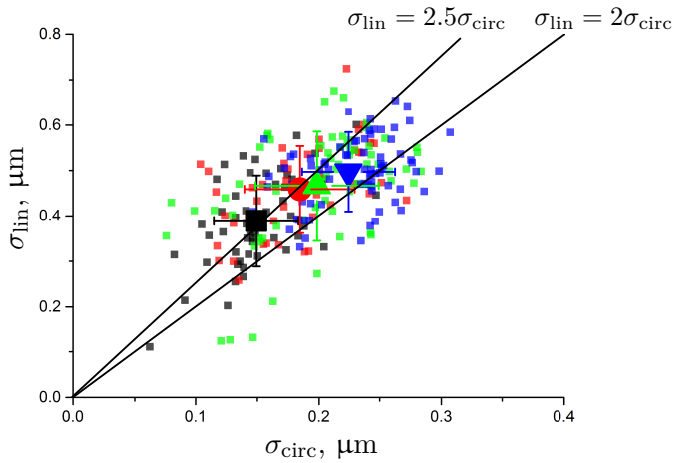

Figure 5.3: Standard deviations of the equilibrium extension for circular (x-axis) and linear (y-axis) configurations of DNA. Each small data point represents a single molecule confined to $150 \times 100\,\mathrm{nm}^2$ channels in 2.5×TBE (blue), 0.5×TBE (green), and 0.1×TBE (red). Black squares correspond to $100 \times 100\,\mathrm{nm}^2$ channels in 0.05×TBE. The large symbols represent the average and standard deviation of all data at a given condition. The solid lines show the relations $\sigma_{\rm lin} = 2\sigma_{\rm circ}$ and $\sigma_{\rm lin} = 2.5\sigma_{\rm circ}$, see Eqs. (5.8),(5.14).

for a narrow range of channel sizes, and only at high ionic strengths. It is therefore not surprising that our measurements do not indicate the presence of the backfolded Odijk regime.

5.3 Quantitative comparisons in the extended de Gennes regime

Paper [IV] consists of a quantitative comparison between experimental measurements of the equilibrium statistics of channel-confined linear DNA, and the predictions of Paper [II]. As such, it is both a test of the predictions of Paper [II] and of the theories describing the physical parameters of DNA (L, $\ell_{\rm K}$, $w_{\rm eff}$). See Chapter 2 for a description of those theories.

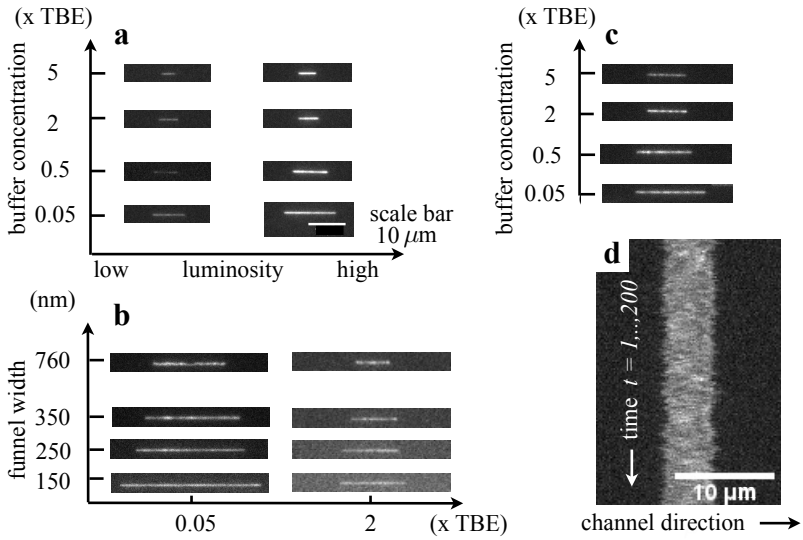

Figure 5.4: **a** Experiment 1. λ-DNA in a 150 nm × 108 nm channel, different buffer concentrations, and different luminosities corresponding to different dye loadings. Shown are representative video frames (scale bar applies to panels **b**,**c** as well). **b** Experiment 2. T4-DNA in a nanofunnel in 0.05× and 2×TBE solution, varying funnel width D_W at constant $D_H = 120$ nm. **c** Experiment 3. T4-DNA in a 302 nm× 300 nm channel, different buffer concentrations. **d** Kymograph of the fluorescence intensity for λ-DNA in a 150 nm×108 nm channel in 5×TBE solution, centre-of-mass motion subtracted.

5.3.1 Experimental method

The experimental data are obtained by measuring the extension of single DNA molecules in nanochannels under three different experimental setups [Fig. 5.4(a) to (c)]. The main purpose of the first experiment is to test the effect of changing the dye load on the extension statistics. The second experiment tests how the extension statistics depend on the channel width D_W. Finally the third experiment is designed to fulfil the conditions for the extended de Gennes as well as possible, thereby allowing a quantitative comparison between the experimental measurements and the predictions of Eqs. (4.23)–(4.24).

The first experiment is a re-analysis of data presented in Ref. [103]. In this experiment [Fig. 5.4(a)], λ-DNA (48502 base pairs) is inserted

into a nanochannel of height $D_{\mathrm{H}} = 150\,\mathrm{nm}$ and width $D_{\mathrm{W}} = 108\,\mathrm{nm}$.[3] DNA extensions are measured at four different buffer conditions (0.05×, 0.5×, 2×, and 5×TBE) and at different dye loads.

In experiment 2 [Fig. 5.4(b)], T4-DNA (165647 base pairs) is inserted into a nanofunnel, with fixed height $D_{\mathrm{H}} = 120\,\mathrm{nm}$ and gradually changing width from $D_{\mathrm{W}} = 92\,\mathrm{nm}$ to $D_{\mathrm{W}} = 815\,\mathrm{nm}$ over a length of $500\,\mu\mathrm{m}$. These experiments are at two different buffer concentrations (0.05× and 2×TBE).

In experiment 3 [Fig. 5.4(c)], T4-DNA is inserted into a channel with $D_{\mathrm{W}} = 302$ nm, $D_{\mathrm{H}} = 300$ nm. The measurements are performed at four buffer conditions (0.05×, 0.5×, 2×, and 5×TBE).

5.3.2 Results

Our results are shown in Fig. 5.5. In panels (a), (c), (e) we plot two theoretical curves for the mean extension. The solid curves uses the actual channel size $D_{\mathrm{H}} \times D_{\mathrm{W}}$. The dashed curves attempts to compensate for the repulsive interaction with the negatively charged walls [2], by using an approximate effective channel size $(D_{\mathrm{H}} - w_{\mathrm{eff}}) \times (D_{\mathrm{W}} - w_{\mathrm{eff}})$. It is not known how accurate this approximation is.[4]

The results of experiment 1 are shown in panels (a) and (b). At low relative luminosity (small dye-to-base-pair ratio) the average extension is well described by Eq. (4.23). For the standard deviation there are larger differences between experiment and Eq. (4.24). By contrast, both observables are overestimated at high ionic strengths and high dye loads. A simple explanation would be that the persistence length decreases slightly with increasing dye load, in agreement with Ref. [61] though not with Ref. [60].

The results of experiment 2 are shown in panels (c), (d). We see that how the average extension depends on D_{W} agrees well with the theoretical prediction. However, the model predictions underestimate

[3] The experimental uncertainties are discussed in paper [IV] and its supplemental material.

[4] In fact, not even the sign of the correction to Eq. (4.23) is obvious, as one effect of violating the condition $D_{\mathrm{H}} \gg \ell_{\mathrm{K}}$ is that density of polymer segments is no longer given by Eq. (4.16). Instead, segments are more evenly distributed throughout the channel [104], which leads to a smaller extension than predicted by Eq. (4.23), i.e. in the opposite direction to the effect of the repulsive interaction between the DNA and the channel walls.

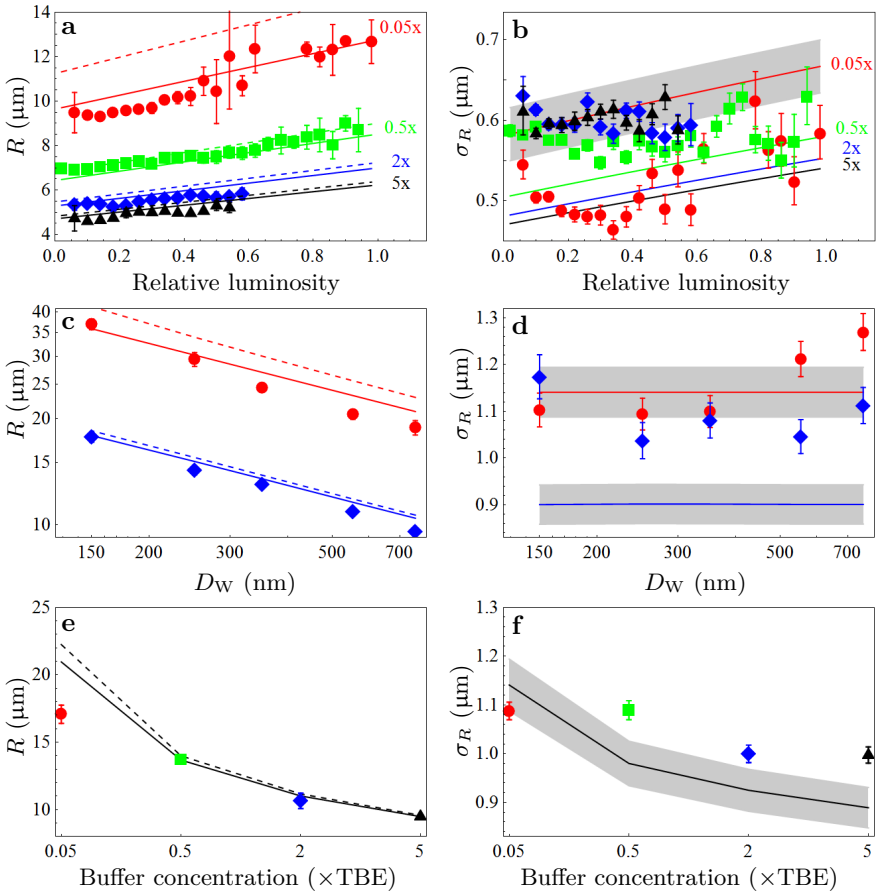

Figure 5.5: Experimental results for 0.05×TBE (red ○), 0.5×TBE (green □), 2×TBE (blue ◊), and 5×TBE (black △) (a), (b) Experiment 1. Mean and standard deviation of the extension of λ-DNA in a narrow nanochannel, as a function of relative luminosity. Theory [Eq. (4.23)], solid lines. The rigorous bounds on the prefactor in Eq. (4.24) are indicated as a shaded region for 0.05×TBE, they are of the same order for the other cases. The corresponding uncertainty for the extension is much smaller and not shown. The dashed line shows theory corrected for wall repulsion (see text). (c), (d) Experiment 2. Same, but for T4-DNA in a nanofunnel with varying width D_W. Note that panel (c) is a log-log plot. (e), (f) Experiment 3. Same, but for T4-DNA in a wider square nanochannel, as a function of buffer concentration (x×TBE). Error bars correspond to 95% confidence intervals from the statistical analysis, the experimental uncertainty is not taken into account.

the standard deviation for the larger ionic strength, and for the largest channel at the lower ionic strength.

Since the condition $D_H \gg \ell_K$ is not satisfied, or only weakly satisfied, it is not surprising that experiments 1 and 2 are not in perfect agreement with Eqs. (4.23)–(4.24). In Paper [IV] we discuss the expected deviations and show that the experimental measurements are in qualitative agreement with expectations.

The results of experiment 3 are shown in panels (e), (f). Simulations indicate [83, 85] that for this channel size, the average extension should be well described by the predictions for the extended de Gennes regime. However, indirect simulations [A, 83] indicate that Eq. (4.24) underestimates the standard deviation by approximately 10% for this channel size.

We find that for the three largest ionic strengths, measurements are in excellent agreement with expectations. The mean extension [panel (e)] agrees very well with the theoretical prediction of Eq. (4.23), and Eq. (4.24) underestimates the standard deviation [panel (f)] by about 10%, just as suggested by simulations.

By contrast, the measurements at 0.05×TBE do not agree with theoretical predictions. Both mean and standard deviation are smaller than expected. The simplest interpretation is that Dobrynin's formula [Eq. (2.6)] overestimates the persistence length in this regime. Note however that measurements at such low ionic strengths are complicated by the fact that it is difficult to achieve uniform dye staining under these conditions.

Fig. 5.6 also shows a comparison between experiment 3 and Eqs. (4.23)–(4.24), this time using not only Dobrynin's formula for ℓ_P, but also Manning's expression, and the prediction from OSF theory (see Section 2.1 and Fig. 2.3). Fig. 5.6 shows that no matter which expression for ℓ_P is used, the mean extension is overestimated at low ionic strengths. The disagreement is significantly smaller when using OSF theory instead of Dobrynin's formula, but on the other hand OSF theory disagrees more with experimental measurements at higher ionic strength, where the measurements are more reliable.

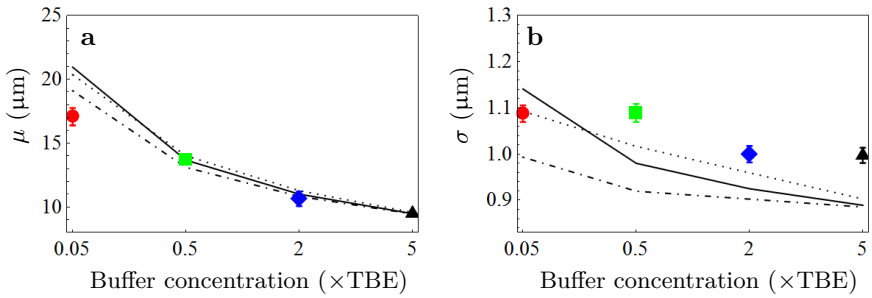

Figure 5.6: A comparison of different theories for the persistence length (see Section 2.1 and Fig. 2.3). Symbols: Same experimental measurements as in Fig. 5.5(e)–(f). Lines: Predictions for the extension statistics [Eqs. (4.23)–(4.24)], using different theories for ℓ_P. Solid line: Dobrynin's expression, Eq. (2.6). Dotted line: Manning's theory, Eq. 25 of Ref. [51]. Dash-dotted line: OSF theory, Eq. (2.5).

5.4 Summary

In Paper [III] we compare the extension statistics of circular and linear DNA confined to channels at the boundary between the Odijk and extended de Gennes regime. The extension statistics of linear polymers in these regimes are known to high accuracy [II, 87], yet little is known about the extension statistics of circular polymers. In Paper [III] we derive approximate expressions for how the mean and standard deviation of the extension of a circular polymer are related to the same observables of a linear polymer. We find that the experimental measurements are consistent with our theoretical expressions, in that the results are intermediate between the predictions in the two regimes, with measurements under more extended conditions closer to the prediction of the Odijk regime, and vice versa.

Paper [IV] tests the predictions of Paper [II]. We find that at high ionic strengths, experimental measurements for the extension statistics of confined DNA agree with the predicted values to within a few percent, using standard theories for the physical parameters of DNA. Further, measurements in a tapered channel (or nanofunnel) qualitatively confirm the functional dependence of the extension statistics on the channel width. However, we find that the agreement between theory and experiments is not as good at low ionic strengths, which might indicate that the

parameters of DNA deviate from theoretical predictions in this regime.

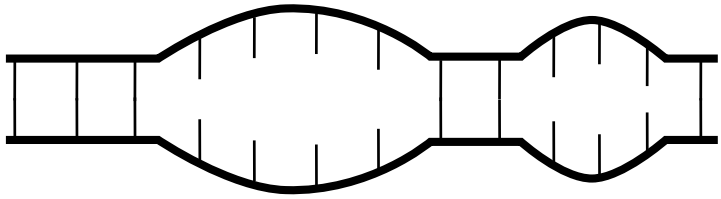

Figure 6.1: Illustration of the Poland-Scheraga model, showing a cartoon of a partially molten DNA molecule as a sequence of bound and unbound regions.

Chapter 6. DNA melting

If the temperature of a DNA molecule is increased significantly above physiological temperatures, some of the hydrogen bonds between the two strands will break, forming local bubbles of single-stranded DNA. This process is referred to as (partial) DNA melting or DNA denaturation [2]. It is illustrated schematically in Fig. 6.1.

Recently there have been a number of studies on the melting of DNA molecules confined to nanochannels [4, 6, 105, 106]. These studies are motivated by the possibility of distinguishing between different DNA sequences by observing the pattern of bound and unbound base pairs. These patterns are related to the underlying DNA sequence since `A-T`–bonds are easier to break than `G-C`–bonds.

However, the analysis of the 'melting curves' obtained in these studies is based on a statistical theory which does not consider the effect of nanochannel confinement on the melting probability. Yet such confinement strongly affects the configurational statistics of the molecule. Therefore it is important to determine what effect it has on the statistics of the melting transition.

Paper [V] analyses the effect of nanochannel confinement on the melting statistics of a highly idealised model of DNA. We find that for this model, even weak channel confinement has a strong impact on the melting statistics. To wit, the transition from the intact, double-stranded state to the fully melted state is much more gradual when the polymer is confined.

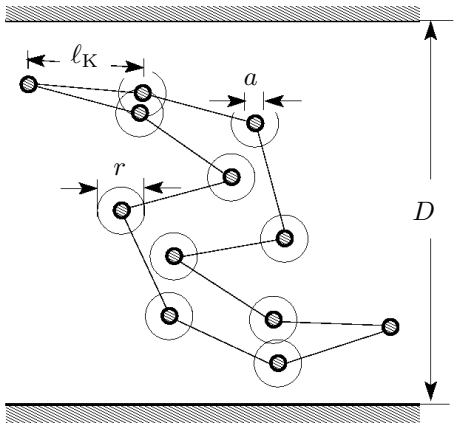

Figure 6.2: Schematic illustration of the three-dimensional model of a confined double- stranded chain that is used in the Monte-Carlo simulations, see text. Note that the two strands are clamped at the ends.

6.1 Model of DNA

The polymer model that we used in Paper [V] is illustrated in Fig. 6.2. The polymer consists of two strands, joined at both ends. Each strand consists of a freely jointed chain of N spherical beads of diameter a, connected by ideal rods of length ℓ_K. For a given monomer n and its partner $n' = n$ (for $1 < n = n' < N$) we test whether the distance between the two monomers is less than r. If so the two monomers are considered bound, and a negative binding energy $-E_b$ (in units such that $k_B T = 1$) is assigned to this pair.

This model disregards a number of important features of DNA, in particular the sequence dependence of the binding energy and the difference in stiffness between double- and single-stranded DNA. Hence it cannot yield any quantitative predictions. Yet for the same reason it is simple to simulate and, in the special case of ideal chains ($a = 0$), amenable to analytical calculations.

6.2 The Poland-Scheraga model of melting

The basic model that we use to describe the statistics of melting was proposed by Poland and Scheraga in 1966 [107]. Consider the double-stranded polymer as a sequence of bound and unbound regions, as

illustrated in Fig. 6.1. The basic assumption of the Poland-Scheraga model is that the different regions do not interact with each other, so that the statistical weight of a configuration is simply the product of the statistical weights of each region.

Within the Poland-Scheraga model, how does the fraction N_b/N of bound base pairs depend on the parameters r, a, D, and E_b? For constant N, this is a difficult question to answer. Yet allowing N to fluctuate in a grand canonical ensemble simplifies the problem immensely [108]. In the thermodynamic limit $\langle N\rangle \to \infty$, averages computed in the two ensembles are expected to agree. The fraction of bound monomers is therefore usually computed in the grand canonical ensemble and evaluated in the thermodynamic limit. This trick allows one to obtain a relatively simple expression for the fraction of bound base pairs of a long chain.

In the grand canonical ensemble, each bound and unbound region can grow or shrink independently of any other. Any given configuration consists of k unbound regions and $k+1$ bound regions. The grand canonical partition function for the system can be calculated by summing over all possible values of k,

$$\mathcal{Z} = \mathcal{Z}_\mathrm{b} + \mathcal{Z}_\mathrm{b}\mathcal{Z}_\mathrm{u}\mathcal{Z}_\mathrm{b} + \mathcal{Z}_\mathrm{b}\mathcal{Z}_\mathrm{u}\mathcal{Z}_\mathrm{b}\mathcal{Z}_\mathrm{u}\mathcal{Z}_\mathrm{b} + \ldots \tag{6.1}$$

$$= \mathcal{Z}_\mathrm{b}\sum_{k=0}^{\infty}(\mathcal{Z}_\mathrm{u}\mathcal{Z}_\mathrm{b})^k = \frac{\mathcal{Z}_\mathrm{b}}{1-\mathcal{Z}_\mathrm{b}\mathcal{Z}_\mathrm{u}}. \tag{6.2}$$

Here $\mathcal{Z}_\mathrm{b}$ and $\mathcal{Z}_\mathrm{u}$ are the grand canonical partition functions of a bound and unbound region, respectively given by

$$\mathcal{Z}_\mathrm{b}(E_\mathrm{b},\mu) = \sum_{m=1}^{\infty}\Omega_\mathrm{b}(m)e^{(E_\mathrm{b}+\mu)m}, \tag{6.3}$$

$$\mathcal{Z}_\mathrm{u}(\mu) = \sum_{m=1}^{\infty}\Omega_\mathrm{u}(m)e^{\mu m}. \tag{6.4}$$

$\Omega_\mathrm{b}(m)$ and $\Omega_\mathrm{u}(m)$ denote the number of different ways to create an bound and unbound region of m base pairs, and μ is the chemical potential (also in units such that $k_\mathrm{B}T = 1$). From this expression for the grand canonical partition function, one can compute the expectation values $\langle N_\mathrm{b}\rangle$ and $\langle N\rangle$ by differentiating $-\log\mathcal{Z}$ with respect to E_b and μ, respectively. In particular, the fraction of bound base pairs is given

by

$$\frac{\langle N_\mathrm{b}\rangle}{\langle N\rangle} = \frac{\partial_{E_\mathrm{b}} \mathcal{Z}_\mathrm{b}}{\partial_\mu \mathcal{Z}_\mathrm{b} + \mathcal{Z}_\mathrm{b}^2 \partial_\mu \mathcal{Z}_\mathrm{u}}. \tag{6.5}$$

This order parameter can be interpreted as the probability that a given monomer is in the bound state. Since we are interested in the thermodynamic limit, the average must be evaluated at the chemical potential μ^* such that $\langle N\rangle$ diverges. This is the case when

$$\mathcal{Z}_\mathrm{b}(\mu^*)\mathcal{Z}_\mathrm{b}(\mu^*) = 1. \tag{6.6}$$

6.3 Effect of confinement

We have seen that computing the fraction of bound base pairs requires one to compute $\Omega_\mathrm{b}(m)$ and $\Omega_\mathrm{u}(m)$. For the ideal case of our model ($a = 0$, no self-avoidance) we do this as follows: For the bound state, we estimate $\Omega_\mathrm{b} \approx c^{2m} p^m K(m)$. Here c is the number of ways in which a single Kuhn length segment can be oriented. For a spatially continuous model such as ours, it is in principle infinite. Imagine that space is finely discretised. Then c is finite and we can show that c drops out in the final result. Further

$$p = P\left(|\mathbf{r}_k - \mathbf{r}'_k| < r \mid |\mathbf{r}_{k-1} - \mathbf{r}'_{k-1}| < r\right)$$

is the probability that monomer k is bound, given that monomer $k-1$ is bound, and $K(m)$ is the probability that a chain of length m does not leave the channel. This probability can be determined from the solution to a diffusion equation [B, 94]:

$$K(m) \approx \exp\left[-\pi^2 \ell_\mathrm{K}^2 m/(3D^2)\right]. \tag{6.7}$$

For the unbound state, we find $\Omega_\mathrm{u} \approx c^{2m} K(m)^2 f(m)$. The factor $K(m)$ is squared since both strands of the unbound region must stay within the channel. The function $f(m)$ is the probability that the two chains form a single closed loop, or alternatively the probability that the random walk performed by the separation $\mathbf{r}_k - \mathbf{r}'_k$ first returns to within a radius r of the origin after m steps. The function $f(m)$ is sketched in Fig. 6.3. For small values of m the probability $f(m)$ is simply the first-return probability for an unconfined three-dimensional random walk

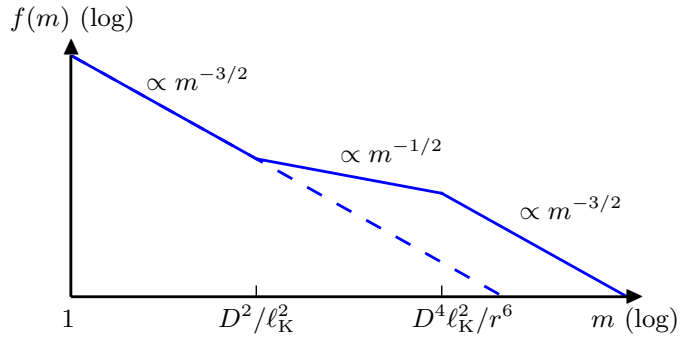

Figure 6.3: A sketch of the first-return probability $f(m)$. Dashed line: $f(m)$ for an unconfined DNA molecule. Solid line: $f(m)$ for ideal DNA confined to a square channel of size $D \gg \ell_K$.

– a short loop does not feel the presence of the walls. Assuming that $m \gg 1$, the first-return probability scales as $f(m) \propto m^{-3/2}$ in this region [109]. In the second and third regions the problem is essentially one-dimensional. Whenever the z-coordinates of the two monomers agree, there is a constant probability $\kappa \propto r^3/(D^2\ell_K)$ that the three-dimensional random walk returns to within a radius r of the origin [II, B]. The probability of first return can therefore be mapped to the solved problem of finding the probability of absorption for a one-dimensional random walk with a partially absorbing sink at the origin [110]. One finds that this probability scales as $f(m) \propto m^{-1/2}$ for small m, and as $f(m) \propto m^{-3/2}$ for large m. In summary, the function $f(m)$ has the form sketched in Fig. 6.3.

Since $\Omega_b(m)$ is a pure exponential, and common exponential factors in Ω_b and Ω_u are of no physical significance[1] it is only the ratio Ω_u/Ω_b which influences the melting probability. The logarithm of this ratio can be interpreted as the difference in entropy between the bound and unbound state. The calculations above show that it is given by

$$\Delta S/k_B = \log \frac{\Omega_u}{\Omega_b} = \alpha + \gamma m - \frac{\pi^2 \ell_K^2 m}{3D^2} + \log f(m). \qquad (6.8)$$

Here α and γ are undetermined constants which do not depend on whether the DNA is confined. The parameter α depends on the undetermined prefactors in our expressions for Ω_b and Ω_u, and $\gamma = \log(1/p)$.

[1] A common exponential factor in Eqs. (6.3)–(6.4) can be eliminated by adding a constant offset to μ.

A final simplification of the calculations is afforded by observing that the terms that are proportional to m have the same effect as shifting the binding energy according to $\epsilon = E_\mathrm{b} - \gamma + \pi^2 \ell_\mathrm{K}^2 m/(3D^2)$.

We have now assembled all the components necessary to compute the fraction of bound base pairs for a long chain. Thus inserting our expressions for Ω_b and Ω_u into Eqs. (6.3)–(6.6) yields (after some simplifications) a closed system of equations for $\langle N_b \rangle \,/\, \langle N \rangle$:

$$\langle N_b \rangle \,/\, \langle N \rangle = [1 + \mathrm{e}^{\epsilon+\mu^*} \mathcal{Z}'_\mathrm{u}(\mu^*)]^{-1} \,, \tag{6.9a}$$

$$\mathcal{Z}_\mathrm{u}(\mu^*) = \mathrm{e}^{\alpha} \sum_{m=1}^{\infty} \mathrm{e}^{m\mu^*} f(m) \,, \tag{6.9b}$$

$$1 = \mathrm{e}^{\epsilon+\mu^*} [1 + \mathcal{Z}_\mathrm{u}(\mu^*)] \,. \tag{6.9c}$$

Here $\mathcal{Z}'_\mathrm{u} \equiv \partial_\mu \mathcal{Z}_\mathrm{u}$. If Eq. (6.9c) admits no solution for real μ^*, then $\langle N_b \rangle \,/\, \langle N \rangle = 0$.

Eqs. 6.9 show that the effect of confinement upon the order parameter is determined by $f(m)$. What does the shape of this function sketched in Fig. 6.3 imply for the melting transition? At high values of ϵ, Eq. (6.9c) yields $\mu^* \approx -\epsilon \ll 0$. For such large negative values of μ^*, the sum in Eq. (6.9b) converges rapidly. The physical interpretation is that the formation of large molten loops is very unlikely when E_b is large. The order parameter is therefore determined by the behaviour of $f(m)$ for small values of m. Yet here $f(m)$ is not influenced by confinement as Fig. 6.3 shows. In this region, then, confinement influences the melting curve only very slightly. In the opposite limit of negative values of ϵ, the fact that $f(m)$ is significantly larger for the confined chain at large m implies that Eq. (6.9c) admits solutions for a larger range of binding energies, and thus that p_b increases at lower energies for the confined chain, compared to the unconfined one. At intermediate binding energies, the binding probability depends sensitively on the exact shape of $f(m)$, and is therefore hard to predict. But we can directly conclude that the melting curve is sharper for the unconfined chain, and smoother for the confined one.

6.3.1 Order of the phase transition

The melting transition of DNA is commonly discussed in terms of the order of the phase transition, which is determined by the scaling of $f(m)$ in the limit $m \to \infty$ [108]. Since $f(m) \propto m^{-3/2}$ both in the confined and

unconfined case, one can conclude that the order of the phase transition is unchanged by channel confinement. Yet as we show above, the melting transition is strongly influenced by confinement. We infer that the order of the melting transition describes only a minute range of temperatures, whereas the overall shape of the temperature dependence of the order parameter depends strongly on the value of the first-return probability for smaller loops.

Note also that the conclusion that the order of the phase transition is unchanged by channel confinement hinges on the fact that Ω_{u} is proportional to the first return probability, rather than the ordinary return probability of a random walk. This is because for the confined polymer, there are far fewer ways to make a single large loop than many smaller ones. This distinction has not been made in previous studies of the melting of DNA. For *unconfined* DNA the order of the melting transition is correctly obtained using the return probability, because the return probability and the first return probability of a three-dimensional random walk decay with the same power [109]. But the difference between return probability and first return probability is crucial for determining the order of the melting transition for confined chains.

6.3.2 Comparison to simulations

Fig. 6.4 shows how confinement influences the melting transition of the simulated system. We plot the probability that the middle base pair is closed, as a function of the binding energy E_{b}. We find that confinement does not influence the melting probability at large E_{b}, but also that increasing confinement leads to a smoother transition overall. These results are in perfect agreement with the theoretical expectations discussed above.

We also show that the melting curve of Fig. 6.4 can be well described by a numerical solution to Eqs. (6.9). For this numerical solution, we assume that $f(m) = (m + A)^{-3/2} + \lambda m^{-1/2} \ell_{\mathrm{K}}^2 / D^2$. This function is consistent with the shape shown in Fig. 6.3, except that it lacks the third regime, where $f(m) \propto m^{-3/2}$ as $m \to \infty$. This is by design, as the simulated chains are too short to exhibit this regime. Details about the fitting procedure are described in Paper [V]. That the numerical solution does not exactly match the simulations is to be expected, as the function $f(m)$ is only approximately correct. Note also that whereas the theoretical curve for the unconfined chain shows a kink at low binding

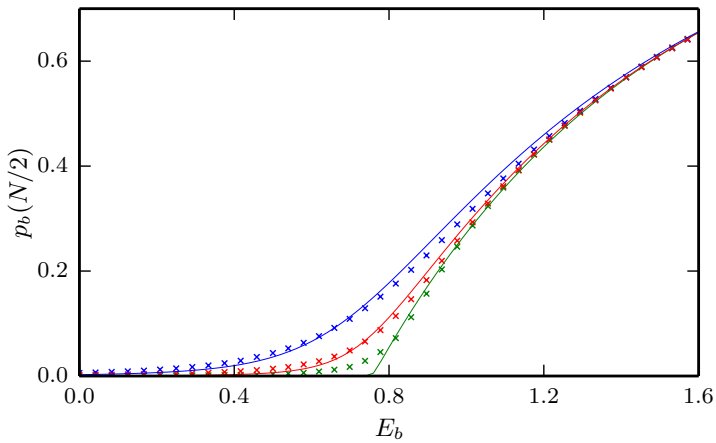

Figure 6.4: The probability $p_\mathrm{b}(N/2)$ that the middle base pair is bound as a function of the binding energy, for an ideal chain with binding energy $E_\mathrm{b} = 0.78$ at different levels of confinement: $D/\ell_\mathrm{K} = 8$ (blue), $D/\ell_\mathrm{K} = 14$ (red), unconfined (green). $N = 400$, $a = 0$, $r = \ell_\mathrm{K}$. Symbols: Results from simulations. Solid lines: Solution to Eqs. (6.9).

energies, the simulated curve is smooth. This discrepancy is caused by the finite size of the simulated system.

6.3.3 Effect of self-avoidance

For the case of self-avoiding chains we have no theoretical predictions. However, we have performed simulations of the model described above with $a = 0.63\ell_\mathrm{K}$. The results are shown in Fig. 6.5. This figure shows that confinement has the same qualitative effect here as for the ideal chain, in that it makes the transition smoother. Yet the effect is even more noticeable in this case. Note that for the case of the unconfined chain (green curve), the transition is sharper than for an ideal chain [see Fig. 6.4]. This is in agreement with established theory for unconfined chains [111, 112].

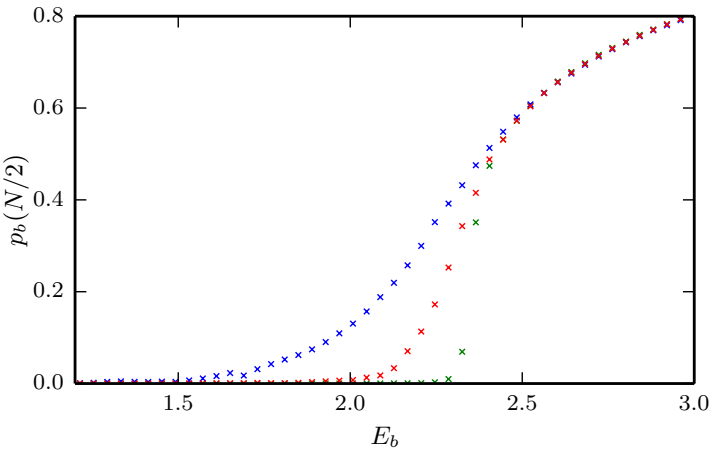

Figure 6.5: The probability $p_{\mathrm{b}}(N/2)$ that the middle base pair is bound as a function of binding energy, for a self-avoiding chain with binding energy $E_{\mathrm{b}} = 2.33$, at different levels of confinement: $D/\ell_{\mathrm{K}} = 8$ (blue), $D/\ell_{\mathrm{K}} = 14$ (red), unconfined (green). $N = 400$, $a = 0.63\ell_{\mathrm{K}}$, $r = \ell_{\mathrm{K}}$.

Part III
Conclusions

Chapter 7. Conclusions

When I made the decision to devote my PhD studies to attempting to understand the statistics of DNA confined in nanochannels there were three aspects of the topic which attracted me especially: First, the hope that these complicated systems could be described by simple models. Second, the possibility to supplement calculations and build intuition by small and simple computer simulations. Third, the prospect that eventual theoretical predictions would be experimentally testable.

Looking back, these three aspects are all evident in the research that I have participated in during my time as a PhD student. Thus the new results of the thesis [I, II, V] follow from modelling a DNA molecule as a string of beads connected by infinitely thin rods, and the calculations have been tested in part by standard Monte Carlo simulations [II, V] and in part by experimental measurements on confined DNA [III, IV].

7.1 Summary of results

In my opinion the most important result of the thesis is the finding of Paper [II], that in the extended de Gennes regime the statistics of a confined polymer can be mapped rigorously to a one-dimensional model, from which both the presence of a universal scaling law and quantitative predictions for the mean and variance of the extension follow. This result is important both because rigorous results are rare for self-avoiding polymers, and because the predictions are of direct experimental relevance.

These predictions are tested in Paper [IV], which finds that experimental measurements on confined DNA agree to within a few percent, using standard theories for the physical parameters of DNA. Intriguingly, the agreement is not as good at low ionic strengths, which might indicate that the parameters which describe DNA deviate from theoretical

predictions in this regime.

Paper [I] fills a gap in the literature on confined semiflexible polymers. While most theoretical and simulation studies of channel-confined polymers have considered square or cylindrical channels, experiments are often performed in rectangular channels. Using standard mean-field theories for the extension statistics of a polymer, we characterise the scaling regimes of a semiflexible polymer in a rectangular channel and show how the extension statistics depend on the height and width of the channel. These predictions are summarised in Tables 4.1–4.2 on pages 28–29.

In Paper [III] we compare the extension statistics of circular and linear DNA confined to channels at the boundary between the Odijk and extended de Gennes regime. In the process we extend the theory for linear polymers in these regimes (discussed in Chapter 4) to the case of circular polymers. We find that the experimental measurements are consistent with a simple interpolation between the theoretical predictions in the two regimes.

Finally, Paper [V] concerns the effect of channel confinement upon the melting of DNA, i.e. the local disassociation between its two strands that can occur at elevated temperatures. This study is motivated by recent studies of DNA melting in nanochannels, and the possibility of using these systems to detect large-scale DNA sequence variations. We solve this problem for a simple model of DNA and find that confinement renders the melting transition smoother, i.e. that the transition from the bound state to the disassociated state occurs over a larger range of temperatures than under unconfined conditions.

7.2 Outlook

The research presented in this thesis leads to a number of new questions which would be interesting to pursue.

The calculations of Ref. [C] indicate that for real DNA the effect of channel confinement on the melting transition is rather subtler than for the model system that we have solved in Paper [V]. Yet since we did not consider the effect of self-avoidance in Ref. [C], the effect of confinement is probably underestimated. In addition, the conclusion rests on the value of an empirical ‘loop factor’ which is not accurately known. Comparing empirical melting statistics to theoretical calculations

of the kind presented in Ref. [C] might allow for improved estimates of this parameter, as well as the other parameters characterising the melting statistics.

Similarly, one of the major complications when attempting a quantitative description of confined DNA is that dependence on the buffer conditions of the persistence length, effective width, and interaction between the molecule and channel walls is not known to high accuracy. Careful comparisons between measurements of the kind presented in Paper [IV] and the theoretical predictions of Paper [II] should in principle allow one to characterise these dependencies. Attempts to measure the DNA parameters in this way could be further facilitated by simulations. Yet one problem when attempting to compare simulations with theory and experiments is that the effective width of common polymer models such as the discrete wormlike chain model [48] does not equal the width of the individual monomer [IV]. Fortunately, it should be relatively straightforward to measure it in simulations, simply by counting the frequency of collisions between two segments enclosed in a fixed volume.

In Paper [III] we compared the extension statistics of a DNA molecule in a circular and linear state. Both in the Odijk and the extended de Gennes regime, the statistics of a linear polymer is known to high accuracy. By contrast, no exact theories exist for circular polymers in these regimes. In Paper [III] we derived approximate expressions for the statistics. However, these derivations could certainly be improved upon. In the extended de Gennes regime, it should be possible to adapt the calculations of the one-dimensional weakly self-avoiding random walk to the case of a circular polymer. One complication which must then be considered is that the one-dimensional model cannot distinguish between knotted and unknotted states of the circular polymer. In the Odijk regime, the major difference between linear and circular polymers is that for linear polymers it is impossible for different segments to overlap, so that it suffices to consider ideal polymers. While self-avoidance probably makes it difficult to obtain exact results for the circular polymer in the Odijk regime, it might be possible to include the effect within a mean-field theory. In general, surprisingly little is known about the extension statistics of circular polymers, considering how common circular DNA molecules are in Nature.

Paper [I] makes a number of predictions for a polymer in rectangular-channel confinement which have yet to be tested in simulations and

experiments. Assuming that such tests confirm the theoretical predictions, it is my belief that the overview of scaling regimes will be of help in the planning and analysis of nanofluidic experiments. If, on the other hand, some of the predictions fail such tests, it will be instructive to understand why mean-field theory fails in these cases.

The most obvious application of the mapping to a one-dimensional model in the extended de Gennes regime [II] is the fact that it proves the exactness of the mean-field scaling for the asymptotic extension statistics and supplies rigorous bounds for the prefactors. However, the mapping to a one-dimensional model and the universal scaling law simplifies the description also of other observables such as correlation functions, finite-size corrections to the scaling laws, and the looping probability of confined DNA.

Additionally, while it is straightforward to show that a similar mapping as in Paper [II] should exist for a polymer confined to a slit, not much is known about the corresponding two-dimensional model. In particular, it is not known whether the two-dimensional model exhibits a similar universal scaling law as the one-dimensional model, nor whether it is possible to prove the correctness of mean-field theories for the polymer confined to a slit using similar techniques as in the one-dimensional case.

Finally, the results of this thesis are solely concerned with equilibrium statistics. Yet some aspects of the theories presented in Papers [I, II] might also be relevant for the study of polymer dynamics. While very little is known about the dynamics of polymers in rectangular confinement [49], it is to be expected that also dynamical properties obey different laws according to which of the scaling regimes sketched in Fig. 4.1 the polymer inhabits. Further, it is interesting to consider whether the mapping to a one-dimensional model [II] could simplify the description of the dynamics in the extended de Gennes regime. For example, the relaxation time of the extension is usually assumed to arise from a balance between a restoring force caused by the increase in free energy as the extension deviates from its mean, and a hydrodynamic friction term [2, 19, 113]. Within this model, the one-dimensional mapping allows for an exact expression of the restoring force term. It is an open question whether the techniques of Paper [II] might allow one to also simplify the description of the friction term, which would lead to an improved understanding of the dynamics of channel-confined DNA.

References

[1] E. Werner. *The distribution and correlations of a polymer confined to a channel*. Licentiate thesis, University of Gothenburg. Göteborg, 2013 (cit. on p. vi).

[2] W. Reisner, J. N. Pedersen, and R. H. Austin. "DNA confinement in nanochannels: physics and biological applications". *Reports on Progress in Physics* **75** (10) (2012), p. 106601. DOI: 10.1088/0034-4885/75/10/106601 (cit. on pp. 1, 9, 27, 40, 48, 53, 66).

[3] B.-Y. Ha and Y. Jung. "Polymers under confinement: single polymers, how they interact, and as model chromosomes". *Soft Matter* **11** (12) (2015), pp. 2333–2352. DOI: 10.1039/C4SM02734E (cit. on p. 1).

[4] W. Reisner, N. B. Larsen, A. Silahtaroglu, A. Kristensen, N. Tommerup, J. O. Tegenfeldt, and H. Flyvbjerg. "Single-molecule denaturation mapping of DNA in nanofluidic channels". *Proceedings of the National Academy of Sciences* **107** (30) (2010), pp. 13294–13299. DOI: 10.1073/pnas.1007081107 (cit. on pp. 1, 53).

[5] F. Persson and J. O. Tegenfeldt. "DNA in nanochannels—directly visualizing genomic information". *Chemical Society Reviews* **39** (3) (2010), p. 985. DOI: 10.1039/b912918a (cit. on pp. 1, 8, 9, 40).

[6] R. L. Welch, R. Sladek, K. Dewar, and W. W. Reisner. "Denaturation mapping of Saccharomyces cerevisiae". *Lab on a Chip* **12** (18) (2012), p. 3314. DOI: 10.1039/c2lc40504k (cit. on pp. 1, 53).

[7] E. T. Lam, A. Hastie, C. Lin, D. Ehrlich, S. K. Das, M. D. Austin, P. Deshpande, H. Cao, N. Nagarajan, M. Xiao, and P.-Y. Kwok. "Genome mapping on nanochannel arrays for structural variation analysis and sequence assembly". *Nature Biotechnology* **30** (8) (2012), pp. 771–776. DOI: 10.1038/nbt.2303 (cit. on p. 1).

[8] P. F. Østergaard, M. Matteucci, W. Reisner, and R. Taboryski. "DNA barcoding via counterstaining with AT/GC sensitive ligands in injection-molded all-polymer nanochannel devices". *The Analyst* **138** (4) (2013), p. 1249. DOI: 10.1039/c2an36522g (cit. on p. 1).

[9] A. R. Hastie, L. Dong, A. Smith, J. Finklestein, E. T. Lam, N. Huo, H. Cao, P.-Y. Kwok, K. R. Deal, J. Dvorak, M.-C. Luo, Y. Gu, and M. Xiao. "Rapid Genome Mapping in Nanochannel Arrays for Highly Complete and Accurate De Novo Sequence Assembly of the Complex Aegilops tauschii Genome". *PLoS ONE* **8** (2) (2013), e55864. DOI: 10.1371/journal.pone.0055864 (cit. on p. 1).

[10] A. N. Nilsson, G. Emilsson, L. K. Nyberg, C. Noble, L. S. Stadler, J. Fritzsche, E. R. B. Moore, J. O. Tegenfeldt, T. Ambjörnsson, and F. Westerlund. "Competitive binding-based optical DNA mapping for fast identification of bacteria - multi-ligand transfer matrix theory and experimental applications on Escherichia coli". *Nucleic Acids Research* **42** (15) (2014), e118–e118. DOI: 10.1093/nar/gku556 (cit. on p. 1).

[11] Y. M. Wang, J. O. Tegenfeldt, W. Reisner, R. Riehn, X.-J. Guan, L. Guo, I. Golding, E. C. Cox, J. Sturm, and R. H. Austin. "Single-molecule studies of repressor–DNA interactions show long-range interactions". *Proceedings of the National Academy of Sciences of the United States of America* **102** (28) (2005), pp. 9796–9801. DOI: 10.1073/pnas.0502917102 (cit. on p. 1).

[12] R. Riehn, M. Lu, Y.-M. Wang, S. F. Lim, E. C. Cox, and R. H. Austin. "Restriction mapping in nanofluidic devices". *Proceedings of the National Academy of Sciences of the United States of America* **102** (29) (2005), pp. 10012–10016. DOI: 10.1073/pnas.0503809102 (cit. on p. 1).

[13] F. Persson, J. Fritzsche, K. U. Mir, M. Modesti, F. Westerlund, and J. O. Tegenfeldt. "Lipid-Based Passivation in Nanofluidics". *Nano Letters* **12** (5) (2012), pp. 2260–2265. DOI: 10.1021/nl204535h (cit. on p. 1).

[14] C. Zhang, D. Guttula, F. Liu, P. P. Malar, S. Y. Ng, L. Dai, P. S. Doyle, J. A. van Kan, and J. R. C. van der Maarel. "Effect of H-NS on the elongation and compaction of single DNA molecules in a nanospace". *Soft Matter* (2013). DOI: 10.1039/c3sm51214b (cit. on p. 1).

[15] M. Roushan, P. Kaur, A. Karpusenko, P. J. Countryman, C. P. Ortiz, S. Fang Lim, H. Wang, and R. Riehn. "Probing transient protein-mediated DNA linkages using nanoconfinement". *Biomicrofluidics* **8** (3) (2014), p. 034113. DOI: 10.1063/1.4882775 (cit. on p. 1).

[16] K. Frykholm, M. Alizadehheidari, J. Fritzsche, J. Wigenius, M. Modesti, F. Persson, and F. Westerlund. "Probing Physical Properties of a DNA-Protein Complex Using Nanofluidic Channels". *Small* **10** (5) (2014), pp. 884–887. DOI: 10.1002/smll.201302028 (cit. on pp. 1, 2, 19).

[17] D. Xia, J. Yan, and S. Hou. "Fabrication of Nanofluidic Biochips with Nanochannels for Applications in DNA Analysis". *Small* **8** (18) (2012), pp. 2787–2801. DOI: 10.1002/smll.201200240 (cit. on p. 1).

[18] J. O. Tegenfeldt, C. Prinz, H. Cao, S. Chou, W. W. Reisner, R. Riehn, Y. M. Wang, E. C. Cox, J. C. Sturm, and P. Silberzan. "The dynamics of genomic-length DNA molecules in 100-nm channels". *Proceedings of the National Academy of Sciences of the United States of America* **101** (30) (2004), pp. 10979–10983 (cit. on pp. 1, 19).

[19] W. Reisner, K. Morton, R. Riehn, Y. Wang, Z. Yu, M. Rosen, J. Sturm, S. Chou, E. Frey, and R. Austin. "Statics and Dynamics of Single DNA Molecules Confined in Nanochannels". *Physical Review Letters* **94** (19) (2005), p. 196101. DOI: 10.1103/PhysRevLett.94.196101 (cit. on pp. 1, 19, 66).

[20] S. Köster, D. Steinhauser, and T. Pfohl. "Brownian motion of actin filaments in confining microchannels". *Journal of Physics: Condensed Matter* **17** (49) (2005), S4091–S4104. DOI: 10.1088/0953-8984/17/49/006 (cit. on pp. 1, 2).

[21] A. Balducci, P. Mao, J. Han, and P. S. Doyle. "Double-Stranded DNA Diffusion in Slitlike Nanochannels". *Macromolecules* **39** (18) (2006), pp. 6273–6281. DOI: 10.1021/ma061047t (cit. on p. 1).

[22] D. Stein, F. H. J. van der Heyden, W. J. A. Koopmans, and C. Dekker. "Pressure-driven transport of confined DNA polymers in fluidic channels". *Proceedings of the National Academy of Sciences* **103** (43) (2006), pp. 15853–15858. DOI: 10.1073/pnas.0605900103 (cit. on p. 1).

[23] A. R. Klotz, L. Duong, M. Mamaev, H. W. de Haan, J. Z. Y. Chen, and W. W. Reisner. "Measuring the Confinement Free Energy and Effective Width of Single Polymer Chains via Single-Molecule Tetris". *Macromolecules* **48** (14) (2015), pp. 5028–5033. DOI: 10.1021/acs.macromol.5b00977 (cit. on p. 1).

[24] F. Persson, P. Utko, W. Reisner, N. B. Larsen, and A. Kristensen. "Confinement Spectroscopy: Probing Single DNA Molecules with Tapered Nanochannels". *Nano Letters* **9** (4) (2009), pp. 1382–1385. DOI: 10.1021/nl803030e (cit. on pp. 1, 19).

[25] C. Zhang, P. G. Shao, J. A. van Kan, and J. R. C. van der Maarel. "Macromolecular crowding induced elongation and compaction of single DNA molecules confined in a nanochannel". *Proceedings of the National Academy of Sciences* **106** (39) (2009), pp. 16651–16656. DOI: 10.1073/pnas.0904741106 (cit. on p. 1).

[26] D. Gupta, J. Sheats, A. Muralidhar, J. J. Miller, D. E. Huang, S. Mahshid, K. D. Dorfman, and W. Reisner. "Mixed confinement regimes during equilibrium confinement spectroscopy of DNA". *The Journal of Chemical Physics* **140** (21) (2014), p. 214901. DOI: 10.1063/1.4879515 (cit. on pp. 1, 7, 9, 19).

[27] W. F. Reinhart, J. G. Reifenberger, D. Gupta, A. Muralidhar, J. Sheats, H. Cao, and K. D. Dorfman. "Distribution of distances between DNA barcode labels in nanochannels close to the persistence length". *The Journal of Chemical Physics* **142** (6) (2015), p. 064902. DOI: 10.1063/1.4907552 (cit. on pp. 1, 7).

[28] S. Köster, J. Kierfeld, and T. Pfohl. "Characterization of single semi-flexible filaments under geometric constraints". *The European Physical Journal E* **25** (4) (2008), pp. 439–449. DOI: 10.1140/epje/i2007-10312-3 (cit. on p. 2).

[29] R. R. Sinden. *DNA Structure and Function*. Elsevier, 2012 (cit. on pp. 3, 4).

[30] O. Kratky and G. Porod. "Röntgenuntersuchung gelöster Fadenmoleküle". *Recueil des Travaux Chimiques des Pays-Bas* **68** (12) (1949), pp. 1106–1122. DOI: 10.1002/recl.19490681203 (cit. on p. 3).

[31] P. J. Hagerman. "Flexibility of DNA". *Annual Review of Biophysics and Biophysical Chemistry* **17** (1) (1988), pp. 265–286. DOI: 10.1146/annurev.bb.17.060188.001405 (cit. on p. 3).

[32] A. Y. Grosberg and A. R. Khokhlov. *Statistical Physics of Macromolecules*. AIP press, 1994 (cit. on pp. 3, 5, 11, 12, 16).

[33] C. G. Baumann, S. B. Smith, V. A. Bloomfield, and C. Bustamante. "Ionic effects on the elasticity of single DNA molecules". *Proceedings of the National Academy of Sciences* **94** (12) (1997), pp. 6185–6190 (cit. on p. 3).

[34] J. F. Marko and E. D. Siggia. "Stretching DNA". *Macromolecules* **28** (26) (1995), pp. 8759–8770. DOI: 10.1021/ma00130a008 (cit. on p. 3).

[35] S. B. Smith, Y. Cui, and C. Bustamante. "Overstretching B-DNA: The Elastic Response of Individual Double-Stranded and Single-Stranded DNA Molecules". *Science* **271** (5250) (1996), pp. 795–799. DOI: 10.1126/science.271.5250.795 (cit. on p. 3).

[36] V. A. Bloomfield. "DNA condensation". *Current Opinion in Structural Biology* **6** (3) (1996), pp. 334–341. DOI: 10.1016/S0959-440X(96)80052-2 (cit. on p. 3).

[37] A. Brunet, C. Tardin, L. Salomé, P. Rousseau, N. Destainville, and M. Manghi. "Dependence of DNA Persistence Length on Ionic Strength of Solutions with Monovalent and Divalent Salts: A Joint Theory–Experiment Study". *Macromolecules* **48** (11) (2015), pp. 3641–3652. DOI: 10.1021/acs.macromol.5b00735 (cit. on pp. 5, 7).

[38] H. H. Strey, R. Podgornik, D. C. Rau, and V. A. Parsegian. "DNA-DNA interactions". *Current Opinion in Structural Biology* **8** (3) (1998), pp. 309–313. DOI: 10.1016/S0959-440X(98)80063-8 (cit. on p. 5).

[39] A. A. Kornyshev, D. J. Lee, S. Leikin, and A. Wynveen. "Structure and interactions of biological helices". *Reviews of Modern Physics* **79** (3) (2007), pp. 943–996. DOI: 10.1103/RevModPhys.79.943 (cit. on pp. 5, 6).

[40] F. Fogolari, A. Brigo, and H. Molinari. "The Poisson-Boltzmann equation for biomolecular electrostatics: a tool for structural biology". *Journal of Molecular Recognition* **15** (6) (2002), pp. 377–392. DOI: 10.1002/jmr.577 (cit. on p. 6).

[41] T. Odijk. "Polyelectrolytes near the rod limit". *Journal of Polymer Science: Polymer Physics Edition* **15** (3) (1977), pp. 477–483. DOI: 10.1002/pol.1977.180150307 (cit. on p. 6).

[42] J. Skolnick and M. Fixman. "Electrostatic Persistence Length of a Wormlike Polyelectrolyte". *Macromolecules* **10** (5) (1977), pp. 944–948. DOI: 10.1021/ma60059a011 (cit. on p. 6).

[43] G. S. Manning. "Limiting Laws and Counterion Condensation in Polyelectrolyte Solutions I. Colligative Properties". *The Journal of Chemical Physics* **51** (3) (1969), pp. 924–933. DOI: 10.1063/1.1672157 (cit. on p. 6).

[44] C.-C. Hsieh, A. Balducci, and P. S. Doyle. "Ionic Effects on the Equilibrium Dynamics of DNA Confined in Nanoslits". *Nano Letters* **8** (6) (2008), pp. 1683–1688. DOI: 10.1021/nl080605+ (cit. on pp. 6, 7).

[45] A. Dobrynin and M. Rubinstein. "Theory of polyelectrolytes in solutions and at surfaces". *Progress in Polymer Science* **30** (11) (2005), pp. 1049–1118. DOI: 10.1016/j.progpolymsci.2005.07.006 (cit. on p. 6).

[46] A. V. Dobrynin. "Effect of Counterion Condensation on Rigidity of Semiflexible Polyelectrolytes". *Macromolecules* **39** (26) (2006), pp. 9519–9527. DOI: 10.1021/ma061030a (cit. on pp. 6, 7, 10).

[47] A. Gubarev, J.-M. Y. Carrillo, and A. V. Dobrynin. "Scale-Dependent Electrostatic Stiffening in Biopolymers". *Macromolecules* **42** (15) (2009), pp. 5851–5860. DOI: 10.1021/ma9008143 (cit. on p. 6).

[48] D. R. Tree, A. Muralidhar, P. S. Doyle, and K. D. Dorfman. "Is DNA a Good Model Polymer?" *Macromolecules* **46** (20) (2013), pp. 8369–8382. DOI: 10.1021/ma401507f (cit. on pp. 7, 65).

[49] D. Gupta, J. J. Miller, A. Muralidhar, S. Mahshid, W. Reisner, and K. D. Dorfman. "Experimental Evidence of Weak Excluded Volume Effects for Nanochannel Confined DNA". *ACS Macro Letters* **4** (7) (2015), pp. 759–763. DOI: 10.1021/acsmacrolett.5b00340 (cit. on pp. 7, 19, 66).

[50] A. Savelyev. "Do monovalent mobile ions affect DNA's flexibility at high salt content?" *Physical Chemistry Chemical Physics* **14** (7) (2012), p. 2250. DOI: 10.1039/c2cp23499h (cit. on p. 7).

[51] G. S. Manning. "The Persistence Length of DNA Is Reached from the Persistence Length of Its Null Isomer through an Internal Electrostatic

Stretching Force". *Biophysical Journal* **91** (10) (2006), pp. 3607–3616. DOI: 10.1529/biophysj.106.089029 (cit. on pp. 7, 51).

[52] D. Stigter. "Interactions of highly charged colloidal cylinders with applications to double-stranded DNA". *Biopolymers* **16** (7) (1977), pp. 1435–1448. DOI: 10.1002/bip.1977.360160705 (cit. on pp. 8, 10).

[53] L. D. Landau and E. M. Lifshitz. *Course of theoretical physics, Vol. 5, Statistical Physics, Part 1*. Third English Edition. Oxford: Pergamon Press, 1980 (cit. on pp. 8, 15).

[54] L. Onsager. "The effects of shape on the interaction of colloidal particles". *Annals of the New York Academy of Sciences* **51** (4) (1949), pp. 627–659 (cit. on pp. 8, 13, 17).

[55] D. Stigter. "Donnan membrane equilibrium, sedimentation equilibrium, and coil expansion of DNA in salt solutions". *Cell biophysics* **11** (1) (1987), pp. 139–158 (cit. on pp. 8, 10).

[56] J. A. Schellman and D. Stigter. "Electrical double layer, zeta potential, and electrophoretic charge of double-stranded DNA". *Biopolymers* **16** (7) (1977), pp. 1415–1434 (cit. on p. 8).

[57] A. Vologodskii and N. Cozzarelli. "Modeling of long-range electrostatic interactions in DNA". *Biopolymers* **35** (3) (1995), pp. 289–296 (cit. on p. 8).

[58] H. S. Rye, S. Yue, D. E. Wemmer, M. A. Quesada, R. P. Haugland, R. A. Mathies, and A. N. Glazer. "Stable fluorescent complexes of double-stranded DNA with bis-intercalating asymmetric cyanine dyes: properties and applications". *Nucleic Acids Research* **20** (11) (1992), pp. 2803–2812. DOI: 10.1093/nar/20.11.2803 (cit. on p. 8).

[59] F. Johansen and J. P. Jacobsen. "1H NMR Studies of the Bis-Intercalation of a Homodimeric Oxazole Yellow Dye in DNA Oligonucleotides". *Journal of Biomolecular Structure and Dynamics* **16** (2) (1998), pp. 205–222. DOI: 10.1080/07391102.1998.10508240 (cit. on p. 9).

[60] K. Günther, M. Mertig, and R. Seidel. "Mechanical and structural properties of YOYO-1 complexed DNA". *Nucleic Acids Research* **38** (19) (2010), pp. 6526–6532. DOI: 10.1093/nar/gkq434 (cit. on pp. 9, 48).

[61] C. U. Murade, V. Subramaniam, C. Otto, and M. L. Bennink. "Force spectroscopy and fluorescence microscopy of dsDNA–YOYO-1 complexes: implications for the structure of dsDNA in the overstretching region". *Nucleic Acids Research* **38** (10) (2010), pp. 3423–3431. DOI: 10.1093/nar/gkq034 (cit. on pp. 9, 48).

[62] A. Sischka, K. Toensing, R. Eckel, S. D. Wilking, N. Sewald, R. Ros, and D. Anselmetti. "Molecular Mechanisms and Kinetics between DNA and

DNA Binding Ligands". *Biophysical Journal* **88** (1) (2005), pp. 404–411. DOI: 10.1529/biophysj.103.036293 (cit. on p. 9).

[63] C. Zhang, F. Zhang, J. A. van Kan, and J. R. C. van der Maarel. "Effects of electrostatic screening on the conformation of single DNA molecules confined in a nanochannel". *The Journal of Chemical Physics* **128** (22) (2008), p. 225109. DOI: 10.1063/1.2937441 (cit. on p. 9).

[64] N. Saitô, K. Takahashi, and Y. Yunoki. "The Statistical Mechanical Theory of Stiff Chains". *Journal of the Physical Society of Japan* **22** (1) (1967), pp. 219–226. DOI: 10.1143/JPSJ.22.219 (cit. on pp. 11, 12).

[65] H. E. Daniels. "The Statistical Theory of Stiff Chains". *Proceedings of the Royal Society of Edinburgh, Section: A Mathematics* **63** (03) (1952), pp. 290–311. DOI: 10.1017/S0080454100007160 (cit. on p. 12).

[66] H. Yamakawa. *Modern theory of polymer solutions*. Harper & Row, 1971 (cit. on pp. 13, 16).

[67] M. Doi and S. F. Edwards. *The Theory of Polymer Dynamics*. Clarendon Press, 1988 (cit. on pp. 13, 15–17).

[68] P.-G. de Gennes. *Scaling Concepts in Polymer Physics*. Cornell University Press, 1979 (cit. on pp. 13, 20, 27, 31).

[69] P. J. Flory. *Principles of Polymer Chemistry*. Cornell University Press, 1953 (cit. on p. 13).

[70] D. W. Schaefer, J. F. Joanny, and P. Pincus. "Dynamics of semiflexible polymers in solution". *Macromolecules* **13** (5) (1980), pp. 1280–1289 (cit. on p. 13).

[71] B. H. Zimm. "Application of the Methods of Molecular Distribution to Solutions of Large Molecules". *The Journal of Chemical Physics* **14** (3) (1946), pp. 164–179. DOI: 10.1063/1.1724116 (cit. on pp. 13, 17).

[72] M. Fixman. "Excluded Volume in Polymer Chains". *The Journal of Chemical Physics* **23** (9) (1955), pp. 1656–1659. DOI: 10.1063/1.1742405 (cit. on p. 15).

[73] Z. Y. Chen and J. Noolandi. "Renormalization-group scaling theory for flexible and wormlike polymer chains". *The Journal of Chemical Physics* **96** (2) (1992), p. 1540. DOI: 10.1063/1.462138 (cit. on p. 16).

[74] Z. Y. Chen and J. Noolandi. "Extended two-parameter theory for flexible polymer chains". *Macromolecules* **25** (19) (1992), pp. 4978–4986. DOI: 10.1021/ma00045a025 (cit. on p. 16).

[75] B. Li, N. Madras, and A. D. Sokal. "Critical exponents, hyperscaling, and universal amplitude ratios for two- and three-dimensional self-avoiding

walks". *Journal of Statistical Physics* **80** (3-4) (1995), pp. 661–754. DOI: 10.1007/BF02178552 (cit. on p. 17).

[76] P. G. De Gennes. "Dynamics of Entangled Polymer Solutions. I. The Rouse Model". *Macromolecules* **9** (4) (1976), pp. 587–593. DOI: 10.1021/ma60052a011 (cit. on p. 18).

[77] C. H. Reccius, J. T. Mannion, J. D. Cross, and H. G. Craighead. "Compression and Free Expansion of Single DNA Molecules in Nanochannels". *Physical Review Letters* **95** (26) (2005), p. 268101. DOI: 10.1103/PhysRevLett.95.268101 (cit. on p. 19).

[78] Y. Kim, K. S. Kim, K. L. Kounovsky, R. Chang, G. Y. Jung, J. J. dePablo, K. Jo, and D. C. Schwartz. "Nanochannel confinement: DNA stretch approaching full contour length". *Lab on a Chip* **11** (10) (2011), p. 1721. DOI: 10.1039/c0lc00680g (cit. on p. 19).

[79] P. Utko, F. Persson, A. Kristensen, and N. B. Larsen. "Injection molded nanofluidic chips: Fabrication method and functional tests using single-molecule DNA experiments". *Lab on a Chip* **11** (2) (2011), p. 303. DOI: 10.1039/c0lc00260g (cit. on p. 19).

[80] Y. Wang, D. R. Tree, and K. D. Dorfman. "Simulation of DNA Extension in Nanochannels". *Macromolecules* **44** (16) (2011), pp. 6594–6604. DOI: 10.1021/ma201277e (cit. on pp. 19, 26).

[81] D. R. Tree, Y. Wang, and K. D. Dorfman. "Mobility of a Semiflexible Chain Confined in a Nanochannel". *Physical Review Letters* **108** (22) (2012), p. 228105. DOI: 10.1103/PhysRevLett.108.228105 (cit. on p. 19).

[82] L. Dai and P. S. Doyle. "Comparisons of a Polymer in Confinement versus Applied Force". *Macromolecules* **46** (15) (2013), pp. 6336–6344. DOI: 10.1021/ma400674q (cit. on pp. 19, 26).

[83] A. Muralidhar, D. R. Tree, Y. Wang, and K. D. Dorfman. "Interplay between chain stiffness and excluded volume of semiflexible polymers confined in nanochannels". *The Journal of Chemical Physics* **140** (8) (2014), p. 084905. DOI: 10.1063/1.4865965 (cit. on pp. 19, 21, 25, 26, 28, 29, 50).

[84] A. Muralidhar, D. R. Tree, and K. D. Dorfman. "Backfolding of Wormlike Chains Confined in Nanochannels". *Macromolecules* **47** (23) (2014), pp. 8446–8458. DOI: 10.1021/ma501687k (cit. on pp. 19, 25, 45).

[85] L. Dai, J. van der Maarel, and P. S. Doyle. "Extended de Gennes Regime of DNA Confined in a Nanochannel". *Macromolecules* **47** (7) (2014), pp. 2445–2450. DOI: 10.1021/ma500326w (cit. on pp. 19, 26, 50).

[86] T. Odijk. "Scaling theory of DNA confined in nanochannels and nanoslits". *Physical Review E* **77** (6) (2008), p. 060901. DOI: 10.1103/PhysRevE.77.060901 (cit. on pp. 21, 25, 26, 28, 29, 45).

[87] T. W. Burkhardt, Y. Yang, and G. Gompper. "Fluctuations of a long, semiflexible polymer in a narrow channel". *Physical Review E* **82** (4) (2010). DOI: 10.1103/PhysRevE.82.041801 (cit. on pp. 21, 25, 29, 43, 51).

[88] T. Odijk. "DNA confined in nanochannels: Hairpin tightening by entropic depletion". *The Journal of Chemical Physics* **125** (20) (2006), p. 204904. DOI: 10.1063/1.2400227 (cit. on p. 21).

[89] L. Turban. "Conformation of confined macromolecular chains: crossover between slit and capillary". *Journal de Physique* **45** (2) (1984), pp. 347–353 (cit. on pp. 23, 27).

[90] T. Odijk. "The statistics and dynamics of confined or entangled stiff polymers". *Macromolecules* **16** (8) (1983), pp. 1340–1344 (cit. on p. 25).

[91] J. Z. Y. Chen. "Free Energy and Extension of a Wormlike Chain in Tube Confinement". *Macromolecules* **46** (24) (2013), pp. 9837–9844. DOI: 10.1021/ma4020824 (cit. on p. 29).

[92] D. R. Tree, W. F. Reinhart, and K. D. Dorfman. "The Odijk Regime in Slits". *Macromolecules* **47** (11) (2014), pp. 3672–3684. DOI: 10.1021/ma500647v (cit. on p. 28).

[93] Z. Benková, P. Námer, and P. Cifra. "Stripe to slab confinement for the linearization of macromolecules in nanochannels". *Soft Matter* **11** (11) (2015), pp. 2279–2289. DOI: 10.1039/C4SM02382J (cit. on p. 29).

[94] E. F. Casassa. "Equilibrium distribution of flexible polymer chains between a macroscopic solution phase and small voids". *Journal of Polymer Science Part B: Polymer Letters* **5** (9) (1967), pp. 773–778. DOI: 10.1002/pol.1967.110050907 (cit. on pp. 29, 56).

[95] R. van der Hofstad, F. den Hollander, and W. König. "Weak interaction limits for one-dimensional random polymers". *Probability Theory and Related Fields* **125** (4) (2003), pp. 483–521. DOI: 10.1007/s00440-002-0248-9 (cit. on pp. 31–33).

[96] F. den Hollander. *Large Deviations*. American Mathematical Soc., 2008 (cit. on p. 32).

[97] R. van der Hofstad, F. den Hollander, and W. König. "Large Deviations for the One-Dimensional Edwards Model". *The Annals of Probability* **31** (4) (2003), pp. 2003–2039 (cit. on p. 32).

[98] R. van der Hofstad. "The constants in the central limit theorem for the one-dimensional Edwards model". *Journal of statistical physics* **90** (5-6) (1998), pp. 1295–1310 (cit. on p. 33).

[99] E. A. DiMarzio. "Proper Accounting of Conformations of a Polymer Near a Surface". *The Journal of Chemical Physics* **42** (6) (1965), p. 2101. DOI: 10.1063/1.1696251 (cit. on p. 33).

[100] F. den Hollander. *Random Polymers*. Springer, 2009 (cit. on p. 36).

[101] R. Van der Hofstad and F. Den Hollander. "Scaling for a random polymer". *Communications in mathematical physics* **169** (2) (1995), pp. 397–440 (cit. on p. 36).

[102] M. A. Tycon, C. F. Dial, K. Faison, W. Melvin, and C. J. Fecko. "Quantification of dye-mediated photodamage during single-molecule DNA imaging". *Analytical Biochemistry* **426** (1) (2012), pp. 13–21. DOI: 10.1016/j.ab.2012.03.021 (cit. on p. 40).

[103] L. Nyberg, F. Persson, B. Åkerman, and F. Westerlund. "Heterogeneous staining: a tool for studies of how fluorescent dyes affect the physical properties of DNA". *Nucleic Acids Research* **41** (19) (2013), e184–e184. DOI: 10.1093/nar/gkt755 (cit. on pp. 44, 47).

[104] J. Z. Y. Chen and D. E. Sullivan. "Free Energy of a Wormlike Polymer Chain Confined in a Slit: Crossover between Two Scaling Regimes". *Macromolecules* **39** (22) (2006), pp. 7769–7773. DOI: 10.1021/ma060871e (cit. on p. 48).

[105] R. Marie, J. N. Pedersen, D. L. V. Bauer, K. H. Rasmussen, M. Yusuf, E. Volpi, H. Flyvbjerg, A. Kristensen, and K. U. Mir. "Integrated view of genome structure and sequence of a single DNA molecule in a nanofluidic device". *Proceedings of the National Academy of Sciences* **110** (13) (2013), pp. 4893–4898. DOI: 10.1073/pnas.1214570110 (cit. on p. 53).

[106] C. Freitag, C. Noble, J. Fritzsche, F. Persson, M. Reiter-Schad, A. N. Nilsson, A. Granéli, T. Ambjörnsson, K. U. Mir, and J. O. Tegenfeldt. "Visualizing the entire DNA from a chromosome in a single frame". *Biomicrofluidics* **9** (4) (2015), p. 044114. DOI: 10.1063/1.4923262 (cit. on p. 53).

[107] D. Poland and H. A. Scheraga. "Occurrence of a Phase Transition in Nucleic Acid Models". *The Journal of Chemical Physics* **45** (5) (1966), pp. 1464–1469. DOI: 10.1063/1.1727786 (cit. on p. 54).

[108] D. Poland and H. A. Scheraga. "Phase Transitions in One Dimension and the Helix—Coil Transition in Polyamino Acids". *The Journal of*

Chemical Physics **45** (5) (1966), pp. 1456–1463. DOI: 10.1063/1.1727785 (cit. on pp. 55, 58).

[109] S. Redner. *A Guide to First-Passage Processes*. Cambridge University Press, 2001 (cit. on pp. 57, 59).

[110] A. Szabo, G. Lamm, and G. H. Weiss. "Localized partial traps in diffusion processes and random walks". *Journal of statistical physics* **34** (1-2) (1984), pp. 225–238 (cit. on p. 57).

[111] M. E. Fisher. "Effect of Excluded Volume on Phase Transitions in Biopolymers". *The Journal of Chemical Physics* **45** (5) (1966), pp. 1469–1473. DOI: doi:10.1063/1.1727787 (cit. on p. 60).

[112] Y. Kafri, D. Mukamel, and L. Peliti. "Why is the DNA denaturation transition first order?" *Physical Review Letters* **85** (23) (2000), p. 4988 (cit. on p. 60).

[113] D. R. Tree, Y. Wang, and K. D. Dorfman. "Modeling the relaxation time of DNA confined in a nanochannel". *Biomicrofluidics* **7** (5) (2013), p. 054118. DOI: 10.1063/1.4826156 (cit. on p. 66).

Part IV
Research papers

Paper I

Scaling regimes of a semiflexible polymer in a rectangular channel

Paper II

Confined polymers in the extended de Gennes regime

Paper III

Nanoconfined Circular and Linear DNA: Equilibrium Conformations and Unfolding Kinetics

Paper IV

Extension of nano-confined DNA: quantitative comparison between experiment and theory

Paper V

Model for melting of confined DNA